Published in final edited form as:
IEEE J Sel Top Quantum Electron. 2012 ; 18(4): 1367–1386. doi:10.1109/JSTQE.2011.2177963.

Diffuse Optical Monitoring of the Neoadjuvant Breast Cancer Therapy

Regine Choe and
Department of Biomedical Engineering, University of Rochester, Rochester, NY, USA; Regine_Choe@urmc.rochester.edu.

Turgut Durduran
ICFO- Institut de Ciències Fotòniques, Mediterranean Technology Park, 08860, Barcelona, Spain; turgut.durduran@icfo.es.

Abstract

Recent advances in the use of diffuse optical techniques for monitoring the hemodynamic, metabolic and physiological signatures of the neoadjuvant breast cancer therapy effectiveness is critically reviewed. An extensive discussion of the state-of-theart diffuse optical mammography is presented alongside a discussion of the current approaches to breast cancer therapies. Overall, the diffuse optics field is growing rapidly with a great deal of promise to fill an important niche in the current approaches to monitor, predict and personalize neoadjuvant breast cancer therapies.

Index Terms

Diffuse optical tomography; diffuse optical spectroscopy; diffuse correlation spectroscopy; diffuse correlation tomography; neoadjuvant therapy; breast cancer; cancer therapy; therapy monitoring; therapy prediction

I. Introduction

Breast cancer is the most frequently diagnosed cancer and the leading cause of cancer death among women worldwide [1]. A report on the global cancer incidences by American Cancer Society estimated 1.4 million new cases of invasive breast cancer and 460,000 cancer deaths for the year 2008 [1]. Five-year survival rate of breast cancer has a wide regional variation: from 89% of the United States to 12% of Gambia. Part of this difference can be attributed to the different availability of advanced cancer detection technologies and treatment options. However, even with advanced technologies and treatments, the prognosis depends heavily on the stage of a cancer at the time of the diagnosis. For example, the 5-year relative survival rate for women with localized breast cancer at the time of diagnosis in the United States is 98%, but the rates for women with a regional stage cancer (i.e., where the cancer cells have already spread to nearby lymph nodes) and a distant stage cancer (i.e., where the cancer cells have spread to distant lymph nodes and other organs) are only 84% and 23% respectively [2]. Clearly, there is still a great deal of need for advances in screening, diagnosis, and therapy.

The current practice of breast cancer treatment planning is based on various factors such as the clinical stage (e.g., Stage 0 to Stage IV, assessed with histopathology and imaging modalities), and tumor estrogen/progesterone receptor (ER/PR) and HER2/neu (human

epidermal growth factor receptor 2; HER2) status [3]. Main approaches are surgery, chemotherapy and radiation therapy with additional hormone therapy (e.g. Tamoxifen or aromatase inhibitors) for ER/PR positive tumors or biologic therapy (Trastuzumab, brand name Herceptin) for HER2 positive tumors.

Unfortunately, it turns out that a patient may not necessarily respond positively to these therapies, presumably due to inter- and intra-subject heterogeneities in tumor biology [4]. Multitude of research efforts are ongoing to identify the physiological origin of this heterogeneity in the therapy response and to develop new types of therapeutic drugs targeting different molecular pathways. While many new oncology drugs are, thus, being developed, it is costly and time consuming to test their effectiveness in phase III randomized clinical trials with thousands of patients and a long-term follow-up [5]. The development of reliable methods to predict the drug response early-on can accelerate this time consuming process to bring new effective drugs to the clinics.

At the moment, there are no accepted methods to predict the therapeutic efficacy. Current candidates for new methods include various biomarkers that can be analyzed from invasively obtained samples such as biopsied tissues or bodily fluids (e.g., blood) or can be imaged *in vivo* using clinical imaging modalities through changes in their morphology or physiology [4]. A key problem for the use of imaging biomarkers in the current clinical practice is that most therapies are administered adjuvantly (i.e., after surgery). Only a few cancer cells would have been left, if any, after surgery, making their detection and characterization prohibitively difficult since resolving a few cells is beyond the spatial resolution of current imaging modalities. In addition, surgery significantly alters the tissue physiology and the surgical effects dominate the images which hinders the interpretation of the images.

Another component of the current treatment plans is neoadjuvant (pre-surgical) chemotherapy which is gaining more acceptance in the clinics. Since it is a pre-surgical therapy, it provides a new opportunity for the use of *in vivo* imaging modalities to identify imaging metrics that can predict the therapy response. This prospect makes the neoadjuvant therapy the emphasis of this review paper which deals with an upcoming new functional imaging modality.

Neoadjuvant chemotherapy was developed to treat locally advanced breast cancer (LABC) in the late 1970s [6] and is now the standard of care for LABC. LABC refers to a large primary lesion (i.e., larger than 5 cm) or a cancer which has spread to the chest wall, the breast skin or to the lymph nodes, but not to other organs. Even with the advances in technology for screening and early-detection, 10-20 % of breast cancers are LABCs in the United States [6]. The primary goal of neoadjuvant chemotherapy was to shrink large primary tumors and render many inoperable patients operable [7]. Initially, the hypothesis was that neoadjuvant chemotherapy would improve the survival compared to adjuvant chemotherapy. However, randomized trials comparing neoadjuvant and adjuvant therapy in operable breast cancer did not find a survival benefit of neoadjuvant therapy, but rather an equivalence to adjuvant chemotherapy [8], [9]. One of the positive findings from these trials was that neoadjuvant chemotherapy was shown to allow more patients to undergo breast-preserving surgery which in turn improved the quality of life for many patients [8]. Based on this, some patients in the stage I or II (i.e., lower stage than LABC) may be allowed to receive neoadjuvant therapy to increase possibility for breast-preserving surgery. Furthermore, complete pathologic response (pCR) to neoadjuvant chemotherapy was determined to be an independent prognostic factor for survival [8]. The determination of pCR status at the surgery enables much faster assessment of therapy than the standard 5-year survival, even though it may not perfectly predict the survival. At least, these positive

findings support that the neoadjuvant therapy platform can be used as an important research tool for new therapy development. Unfortunately, approximately 8-20% of breast cancer patients undergoing neoadjuvant chemotherapy will not have clinical or pathologic response [10], [11]. We hypothesize that this shortcoming could be addressed by the development of newer imaging modalities for the biomarkers of therapeutic efficacy.

From the view of managing an individual patient, the therapy optimization in terms of dosing, timing, and the combination with conventional therapies becomes possible with practical therapy response prediction methods that could readily and reliably be utilized for each patient. In turn, this ability to optimize the treatment for an individual patient can increase the survival and/or quality of life. For example, if non-responders can be identified quickly, ineffective therapies can be discontinued in order to reduce unnecessary side-effects and costs. For the case of partial responders, the therapy response monitoring can help doctors to tailor the treatments to enhance therapeutic effects and the survival rates even further.

Several clinical routine and research imaging modalities such as X-ray mammography, ultrasound, magnetic resonance imaging (MRI) and spectroscopy (MRS), positron-emission tomography (PET), single photon emission computed tomography (SPECT) are being tested for their capabilities to predict the therapeutic efficacy. In addition, new imaging methods like diffuse optical methods are emerging for this application.

Initially, the development of diffuse optical methods for breast cancer was geared towards the diagnosis (i.e., non-invasive differentiation of the malignant tumors from healthy tissue and/or benign lesions) based on the quantification of functional information. Interested readers can find more details on this topic in recent reviews [12]–[16]. Recently, researchers have started to recognize the potential of diffuse optics for therapy monitoring and prediction. This was reviewed in a recent publication in the year 2009 [13], but results are flowing in rapidly and the field has progressed from presenting a few case studies to attempts with medium-sized populations to differentiate response groups. These attempts are promising, but still limited in the number of subjects that were enrolled, and they differ in the definition of responding and non-responding groups. Here, we compile results of these activities and try to unify the definitions for the ease of comparison.

We continue this paper by reviewing the current progress in the development of new clinical imaging modalities for therapy prediction. After this sets the stage for the use of diffuse optical methods for functional imaging, we (very briefly) outline the fundamentals of diffuse optical methods with an emphasis on their applications for breast cancer research. Then, selected case studies demonstrating the sensitivity of diffuse optical methods to changes induced by therapy are presented. Finally, we discuss the feasibility and the future of differentiating the therapy responders from non-responders based on new data from several research groups.

II. Neoadjuvant chemotherapy monitoring with clinical imaging modalities

Currently in the United States, patients undergoing neoadjuvant chemotherapy typically receive three to four cycles of a given chemotherapy regimen followed by another three to four cycles of another regimen. Each cycle is two to three weeks long depending on the regimen. The responses to the chemotherapy are either assessed at the completion of both regimens (e.g., in LABC patients) or after three to four cycles of the initial regimen (e.g., in stage II patients for breast conservation). Depending on the response, the next treatment plan is drawn up. For example, many chemotherapy responders from LABC population receive a combination of surgery (mastectomy or lumpectomy depending on the response), axillary dissection and radiation therapy after completion of chemotherapy. Whereas, non-

responders receive additional chemotherapy and/or neoadjuvant radiation before going into the surgical approach [3].

Even though important therapeutic decisions, such as the above examples, rely on the correct assessment of the present and future tumor response to the therapy, currently no imaging modality has been accepted as the routine method for therapy assessment and prediction. This is despite the fact that many imaging methods are undergoing extensive clinical trials.

In early studies, tumor shrinkage was assessed mostly with clinical palpation. Then, X-ray mammography (main clinical screening modality [17]), and ultrasonography (adjunct imaging modality) were tested for their abilities to monitor neoadjuvant chemotherapy. However, the detection of tumor shrinkage by these modalities is often hampered by therapy-induced fibrosis [18]–[21]. As an alternative approach, more advanced and more expensive modalities, such as standard magnetic resonance imaging (MRI) and dynamic-contrast-enhanced (DCE) MRI demonstrated themselves to be useful for defining the extent of the residual disease [22]–[25]. To put in some concrete numbers, in a prospective comparison study, the agreement between imaging modalities and the pathological assessment as the gold standard was 19% (clinical palpation), 26% (mammography), 35% (ultrasonography) and 71% (DCE-MRI) [26]. For clinical purposes, these are still modest agreement, but place DCE-MRI as the leading potential modality. We note that DCE-MRI is interesting because its contrast relies on increased vascularity and the leakage of the vasculature. Furthermore, tumor volume change between pre and post-therapy determined by DCE-MRI was shown to predict therapy outcome in terms of recurrence-free survival [27]. A multi-center trial sponsored by the American College of Radiology Imaging Network (ACRIN) is ongoing to test MRI as a therapy assessment tool [28], and to use MRI and other biomarkers to test new chemotherapy drugs in an adaptive breast cancer trial design [5].

Positron emission tomography (PET) is another advanced clinical imaging modality being investigated for its potential role for therapy monitoring. Unlike most of the other clinical imaging modalities which depend on anatomical (or morphological) information, PET provides functional information, most often the glucose metabolism using ^{18}F-FDG (Fluorodeoxyglucose). In the clinical settings, at the moment, PET is most useful as a secondary imaging modality when results of other imaging are equivocal, and may reveal locoregional or unsuspected distant disease [29]. Importantly, PET has demonstrated that the metabolic changes of cancer due to cancer therapy can precede the morphological changes and can be detected as early as eight days after initial chemotherapy cycle [30], [31]. Reliable differentiation between responding and non-responding breast cancers with PET as early as after the first cycle of chemotherapy was demonstrated by many investigators [32]. Finally, in a prospective study, PET demonstrated superior performance in predicting pathologic response after two cycles of chemotherapy when compared to ultrasound and mammography [33].

There are several, non-routine imaging modalities that are also being tested. In particular, from a functional viewpoint, magnetic resonance spectroscopy (MRS) and single-photon emission computed tomography (SPECT) stand out. In particular, total choline-containing compounds (tCho) and water-to-fat ratio from proton MRS (^{1}H-MRS) have demonstrated their potential as early indicators of treatment response [34], [35], as early as within 24 hour after initial therapy [36]. Efforts are ongoing to incorporate MRS to MRI examinations [35], but its routine clinical adaptation requires more trials. [Technetium-99m]-Sestamibi pharmacokinetic parameters measured by SPECT were shown to correlate with tumor blood

flow [37], and to predict disease free survival and overall survival [38]. SPECT is difficult to utilize and has not yet been adapted for routine use.

DCE-MRI, PET, MRS and SPECT modalities highlight the potential for hemodynamic and metabolic measurements. However, despite this sensitivity to therapy-induced metabolic changes, they have not yet received clinical acceptance which usually follows after successful randomized clinical trials. Several issues need to be resolved before embarking on expensive clinical trials with these modalities. One of these issues is the standardization of quantification within a given imaging modality [35]. Another problem is that there are no unified response classifications which hinder these trials [39]. Furthermore, there are some social and economic issues related with the intrinsic characteristics of these imaging modalities: they are expensive, non-practical and limited in availability. DCE-MRI, SPECT and PET require the injection of a contrast agent, which introduces the possibility of adverse events. Furthermore, PET and SPECT require the development, synthesis, and injection of radioactive agent which require local facilities to deal with radioactive materials, poses patient safety issues and tough logistical problems due to the limited half-life of the agents. These limit their uses and specifically hinder frequent measurements on the patients, which in turn make the discovery of the optimal time point to differentiate different responding groups very difficult.

This brings us to the question of a promising new paradigm for therapy planning which is the hypothesized potential benefit of frequent monitoring (even daily!) for prescribing customized regimens and to improve the patient well-being during the therapy. The time-scale of metabolic and physiologic therapy responses may vary widely depending on the mechanism of therapeutic drugs as well as the individual tumor biology. While X-ray mammography (with some limitations) and ultrasound may be utilized several times without major health risks, they do not readily provide metabolic information which may be the key-parameter that changes rapidly and often. As was discussed earlier, MRI and PET based modalities are prohibitively expensive and unavailable for such use. Therefore, a non-invasive, inexpensive, non-ionizing-radiation-based detection modality sensitive to metabolic and physiological changes is expected to be of critical importance. This modality could complement frequent ultrasound or X-ray monitoring and few time-point MRI/PET monitoring.

Among many candidates of non-invasively measurable metabolic parameters, hemodynamic parameters have high potential to distinguish different response groups. For example, a reduction of tumor angiogenesis from neoadjuvant chemotherapy in combination with hormone therapy has been confirmed by pathological analysis [40]. Blood flow and flow-related microenvironmental parameters have been known to affect the sensitivity of cancer cells to various cancer therapies such as chemotherapy, radiation therapy to photodynamic therapy [41], [42]. Furthermore, tumors with relatively poor perfusion may not receive adequate delivery of the therapies with systemic injection. Under-perfused tumors may also be hypoxic and tumor hypoxia presents resistancy to radiation therapy, anti-cancer agents and photodynamic therapy-mediated cell death [41], [43].

As was described before, diffuse optical methods are attractive because they provide quantitative physiological information about tumor vascularity, blood flow, blood oxygenation, water, and lipid concentrations [16]. Most importantly, diffuse optical methods are suitable for frequent monitoring since they do not use ionizing radiation and are relatively inexpensive. Although diffuse optical methods have low spatial resolution compared to other imaging modalities, this does not limit their applicability to therapy monitoring, since neoadjuvant chemotherapy is offered to patients with large breast cancers. There could be a concern that the significant change in tumor volume and location may

affect the quantification power of diffuse optical methods (especially ones based on simple analysis). These methods can still be applied for predicting therapy at early stage; the tumor volume change generally takes long time (>1-2 months) compared to the physiological changes that diffuse optics aim to monitor. In the later time point, tumor volume and location information can be incorporated as a correction factor.

A note on the classification of the therapy response

The collective result of the imaging studies is that newer methods still need to be developed and the data should be gathered in a more standardized fashion to be compared. For example, even though, a subpopulation of neoadjuvant chemotherapy patients who achieved complete pathologic responses showed a significant increase in survival time in a randomized clinical trial [8], the exact relationship between the degree of the pathologically determined partial response and the survival rate is still unclear. This also plays a role in the interpretation of the diffuse optical data which we will discuss in detail. The lack of a universal criteria in pathologic response assessment towards classifying responders and non-responders led to variations in the diffuse optical data that has so far been published. In order to clearly describe these different interpretations, we start by defining different degrees of pathologic responses following the one used in reference [44]:

pCR A complete pathologic response (pCR) is defined as not having any residual invasive or *in situ* tumor in the post-treatment biopsy/surgical specimen.

pPR1 A near-complete pathologic response (partial pathologic response of level 1 or pPR1) refers to the case where the remaining residual tumor percentage is less than 10% of the pre-treatment size (i.e., tumor size decrease >90%).

pPR2 A partial pathologic response of level 2 (pPR2) refers to a decrease in the tumor size of more than 50% and less than 90% compared to the pre-treatment size.

pPR3 A partial pathologic response of level 3 (pPR3) is used when the decrease in the tumor size is less than 50%, but greater than 10%.

pPR4 A partial pathologic response of level 4 (pPR4) refers to a minimal response to therapy with more than 90% of the tumor remaining (i.e., tumor size decrease <10%).

While this classification based on the tumor size reduction is useful for this review, in general, one should keep abreast with more sophisticated methods to quantify the treatment outcome which are gaining clinical recognition. One such estimate of treatment outcome is called the “residual cancer burden”, which combines information on the primary tumor and the metastatic involvement of lymph nodes [45].

We now describe the fundamentals of diffuse optics and move on to the progress in the field for neoadjuvant therapy monitoring.

III. Fundamentals of Diffuse Optics

A. An overview of diffuse optics

Diffuse optical probing of tissues is based on the use of light sources and detectors in the near-infrared wavelength regime (λ = 650-1000 nm). In this window of wavelengths, the overall absorption due to main tissue chromophores such as deoxygenated hemoglobin (Hb), oxygenated hemoglobin (HbO_2), water (H_2O), and lipids is relatively small. This limits the light losses, enabling significantly deeper light penetration than visible light and also than light from further regions of the infrared (i.e., mid- to far-infrared) where the water absorption dominates. To give an idea, in the near-infrared window, this absorption length is

about ~200 mm. In the subsequent formalism, the reciprocal of the absorption length which is wavelength dependent is denoted by the absorption coefficient ($\mu_a(\lambda)$).

The second important aspect of the photon propagation in tissues in these wavelengths is that the "scattering length", which corresponds to the typical distance traveled by photons before they scatter, is rather short (~1-100 μm). In general, for deep tissues, since we deal with a very large number of scattering events, a longer "random walk step" (~1 mm) which corresponds to the typical distance traveled by photons before their directions randomize can be utilized for analysis. The formalism utilizes a wavelength (λ) dependent reduced scattering coefficient ($\mu_s'(\lambda)$) which denotes the reciprocal of the photon transport mean free path.

As we can see from these length-scales, the propagation of photons in these wavelengths is dominated by multiple scattering. The key component of the tissue probing by diffuse light is the ability to decouple the absorption and the scattering effects in order to quantify each wavelength dependent coefficient independently [16]. This decoupling is achieved by use of a photon transport model based on the diffusion approximation. Once each parameter is quantified in space and/or time, measurements from multiple wavelengths are utilized to derive estimates of the chromophore concentrations. Figure 1b shows examples of "generic" measurements with estimates of photon visiting probabilities (or probability density function) from a photon diffusion model overlaid which can estimate the volume of tissue visited by the detected photons [46]. To learn more about the technologies and their applications, we refer our readers to various recent reviews [16], [47]–[54].

Note that, herein, we will refer to the measurements that estimate bulk optical and physiological properties based on the assumption that the probed tissue is homogeneous or nearly-homogeneous (e.g. layered) as "spectroscopy" (DOS) and those that spatially resolve the properties in three-dimensions as "tomography" (DOT). The distinction, while not being a sharp one, generally implies differences in analysis algorithms and increased complexity in the instrumentation.

In terms of its implementation, depending on the different source modulation and the corresponding detection electronics, instrumentation techniques can be categorized as continuous-wave (CW), frequency-domain (FD, using sinusoidally intensity-modulated light at radio-frequency), or time-domain (TD, using ~tens of picosecond width light pulse). The information content per single source-detector pair per wavelength is the highest for TD technique, and the lowest for the CW technique. The choice of one method over another depends on the cost and availability of the current technologies, and the algorithms to be deployed [16].

Both "spectroscopy" and "tomography" involve the development of a "forward" model based on the diffusion equation that explains the propagation of the photons through the tissues for a given optical property distribution and source-detector geometry [52]. For a given source type, analytic solutions for fluence rate exist for simple geometries such as homogeneous media without boundaries (infinite), with a single (semi-infinite) or dual (slab) infinite plane boundary between diffuse and nondiffuse media, diffuse-diffuse layers and several others [16]. These "forward" models are then utilized in various fitting algorithms to fit either for the λ dependent absorption and scattering coefficients or for the chromophore concentrations directly. This type of solutions are generally utilized for "spectroscopic" approaches that form the bulk of the example data that is shown in this review.

Figure 1 and Figure 2 illustrate the stand-alone DOT and hand-held DOT/DOS systems that are most commonly utilized. Note that there is a significant difference in the breast volume and shape based on whether the subject lies in the prone (Figure 1a) or supine (Figure 2) position. This difference is used to take advantage of the deformable breast tissue to gain access to the maximal tissue volume possible.

Figure 1b shows a series of illustrations demonstrating photon propagation in the female breast and the importance of physical modeling based on a "generic" parallel plate imaging/spectroscopy geometry with a set of sources (dark arrows) and detectors (light arrows) as shown on the top-middle panel on a DCE-MRI image. A mask (bottom two rows) was then applied indicating high contrast agent uptake ("white"), the breast tissue ("light gray") and elsewhere ("black"). Two different geometries are indicated in the bottom rows; middle-row shows a series of transmission measurements and bottom-row shows reflectance measurements. Using solutions for photon diffusion equation, i.e. numerical simulations, the photon visiting probability (or probability density function) based on the so-called three-point Green's functions [46] is overlaid on the tumor and breast masks. Successful tomography requires accurate modeling of these measurements and incorporation of multiple measurements in an inverse-problem. Spectroscopy, on the other hand, utilizes only a few such measurements and attempts to measure the "bulk" volume at several positions.

Figure 2 depicts the similar information as shown in Figure 1b of reflectance measurements, but in supine measurement position. Both figures illustrate that the the depth of the probed tissue volume is increased as the source-detector separation is increased. However, the supine position enables the flattening of the breast and effectively reduces the tissue depth from the surface. This type of probes are generally scanned across the breast in 2D and sometimes are combined with other modalities.

In general, 3D tomography requires more complex "forward" models. Therefore, often, numerical solutions based on finite difference or element methods are used to solve for arbitrary geometries and heterogeneities [55]. This is then employed in a complex "inverse problem" which refers to the problem of estimating the spatial distribution of $\mu_a(\mathbf{r})$ and $\mu_s'(\mathbf{r})$ based on measurements of fluence rate on the tissue surface (where $\mathbf{r}$ is the position within the 3D space of interest). The DOT inverse problem is intrinsically nonlinear, often involves large data-sets, is ill-posed and computationally intensive. Thus, the class of image reconstruction methods for DOT is an interesting and complex research area on its own [52].

Furthermore, in general, diffuse optical methods can readily be combined with other modalities such as MRI, X-Ray, PET, CT, ultrasound and others. Therefore, some research groups utilize spatial *a priori* information from other conventional imaging modalities (e.g., MRI, ultrasound, X-ray tomosynthesis) within the image reconstruction frame to improve the resolution and accuracy of reconstructed images [56]–[63]. These come with the additional benefit that it makes the the interpretation of the multi-modal data simpler without the need for complex algorithms to re-map the images of different modalities onto a common space [64].

The goal of spectroscopy and tomography is to quantify μ_a and μ_s' either in bulk or at each volume element in 3D at multiple wavelengths. Once they are quantified, the chromophore concentrations are extracted from $\mu_a(\lambda) = log(10)\,\Sigma_i\,\varepsilon_i(\lambda)C_i$ where ε_i and C_i are the extinction coefficient and the concentration of i^{th} chromophore respectively. Based on the concentrations of Hb and HbO_2, total hemoglobin concentration ($THC = C_{HbO2} + C_{Hb}$) and blood oxygen saturation ($StO_2 = C_{HbO2}/THC$) can be derived. In addition, scattering amplitude (A) and power (b or SP in other literature) which depend on scatterer density and

size can be extracted using simplified Mie-scattering approximation, $\mu_s'(\lambda) = A\lambda^{-b}$, of the wavelength dependence of the scattering coefficients. These relationships can also be employed as constraints within the inverse problem framework. In this case, all the wavelengths data are utilized to extract chromophore concentrations and scattering properties without finding out μ_a and μ_s' at each wavelength to address issues such as cross-talk and uniqueness [16].

B. Diffuse correlation spectroscopy & tomography

Diffuse light carries more information when coherent sources are utilized. The speckle fluctuations of the diffused light is sensitive to the motions of the scatterers. In tissues, the dominant contribution of the signal turns out to be from the red blood cells. For biomedical applications, in laser Doppler and laser speckle flowmetry techniques [1], this has mostly been utilized in its single-scattering version where closely spaced source-detector pairs are utilized and the spatial/temporal/spatio-temporal speckle statistics are analyzed [65]–[67]. These technologies have proven themselves to be useful in numerous applications where superficial (i.e., <1 mm deep) tissues can be interrogated and relevant clinical information can be obtained. This approach simplifies the experimental analysis and implementation, but also limits the reliability and the amount of information that can be extracted from real tissue samples. Yodh group at the University of Pennsylvania (where both authors used to be part of) has pioneered the extension of the blood flow measurements based on the laser speckle statistics to deep tissues. This multiple scattering analog of the earlier approaches was named "diffuse correlation spectroscopy" (DCS) [16], [68], [69]. Here, we note that the "diffusing wave spectroscopy" (DWS) [70]–[72] introduced before DCS, and DWS is essentially an integral formulation of DCS. We choose to utilize the name DCS in the biomedical optics field because "DWS" had connotations for both absorption spectroscopy and fluctuation spectroscopy. For recent and detailed reviews of DCS, see references [16], [53].

Briefly, a major step towards the utilization of the multiple scattering approaches to biomedicine was again the development of a photon diffusion equation that describes the transport of the electric field temporal auto-correlation function through turbid media [68], [69]. This approach has unified earlier models [67], [70]–[72] of the spectral broadening experienced by highly scattered light in materials such as colloids, foams and tissues, and enabled the development of theory and instrumentation to optically probe blood flow in thick tissues. Note that the correlation diffusion equation has the similar form as the photon diffusion equation and many of the the theoretical formalism developed for DOS and DOT are easily transferable to DCS and diffuse correlation tomography (DCT) [68], [73], [74].

The correlation diffusion equation describes the electric field temporal auto-correlation function $G_1(\mathbf{r}, \tau) = \langle \mathbf{E}(\mathbf{r}, t) \cdot \mathbf{E}^*(\mathbf{r}, t+\tau) \rangle$ as

$$\left[\nabla \cdot D(\mathbf{r}) \nabla - v\mu_a(\mathbf{r}) - \frac{\alpha v k_0^2}{3} \mu_s' \left\langle \Delta r^2(\tau) \right\rangle \right] G_1(\mathbf{r}, \tau) = -vS(\mathbf{r}). \quad (1)$$

where, $k_0 = 2\pi/\lambda$ is the wavevector of the photons, α is the percentage of moving scatterers, τ is the correlation delay time, and $\langle \Delta r^2(\tau) \rangle$ is the mean-square displacement of scattering particles. The measurable quantity with DCS is not G_1, but the normalized intensity auto-

[1] The overall field is known as "dynamic light scattering" in other contexts.

correlation function $g_2(\mathbf{r},\tau)=\frac{\langle I(\mathbf{r},t)\,I(\mathbf{r},t+\tau)\rangle}{\langle I(\mathbf{r},t)\rangle^2}$. G_1 and g_2 are related through the Siegert relation [75]

$$g_2(\tau)=1+\beta|g_1(\tau)|^2 \quad (2)$$

where β is a constant determined by the collection optics.

In practice, $\mu_a(\mathbf{r})$ and $\mu_s'(\mathbf{r})$ are either assumed to be homogeneous values based on literature, or obtained through solving the photon diffusion equation using DOS or DOT [76]. This readily calls for *hybrid* approaches that combine DCS/DCT with DOS/DOT and many publications have indeed utilized this hybridization [16]. Once the mean-squared displacement is modeled, often as an "effective" Brownian motion as $\langle \Delta r^2(\tau)\rangle = 6D_B\tau$, where D_B is the "effective" Brownian coefficient, a blood flow index (BF) to describe the red blood cells can be obtained as $BF = \alpha D_B$ by solving an inverse problem as outlined for DOS/DOT. There is still a lot of interesting physics to be discovered about the specific models that should be utilized to describe the mean-squared displacement term in Equation 1. For the ongoing research, we refer the readers to references [16], [53], [54], [77], [78].

This combination of DOS and DCS further enables one to estimate the metabolic rate of oxygen (MRO_2) based on THC, StO_2, and BF [16]. It should be noted that BF is not, yet, a robust measure of *absolute* blood flow, but the relative change in BF has been shown to have excellent quantitative agreements with relative values estimated by other methods including laser Doppler flowmetry, transcranical Doppler ultrasound, arterial-spin labeled MRI, Xenon-inhalation CT, fluorescent microspheres and Indocyanine Green wash-in/wash-out dynamics [16], [79] in a wide range of applications and tissues ranging from mice tumors to adult brain. Overall, these validation studies have shown that DCS measurements of blood flow variations are robust and are in good agreement with expectations and with other measurement techniques. We believe that with improved physical modeling and technological advances DCS will become a robust technique even for absolute measures of blood flow in deep tissues.

For "optical mammography", DCS was introduced in the year 2005 [80] where a significant increase of BF in tumors was observed with some preliminary indication that there was a differentiation between benign and malignant tumors. The probed tissue volumes are quite similar to DOS/DOT (Figures 1b & 2) and, in principle, both type of approaches are possible. In practice, however, due to limitations in the current source and detector technologies, DCS has mainly been implemented as a hand-held probe. A recent monograph has included some spectroscopic results in the tandem, transmission geometry which demonstrates that with a better dynamic range it should be possible to construct a stand-alone DOT system [81]. To further illustrate the type of data that is available from a DCS system, Figure 3 shows the measured intensity auto-correlation curves from a "healthy" region in comparison to that from the "tumor" region with the fitted data from the physical model overlaid.

This exciting development from the first results was later followed up by a collaborative study between the UPENN and UCI groups where the DCS device was hybridized with a broad-band DOS device and early responses to chemotherapy was observed [82]. In this review, we take advantage of the fact that both of the authors were involved in the development of DCS to outline the latest, mostly unpublished, developments towards therapy monitoring using DCS and DOS together.

C. Overview of "Diffuse optical mammography" (DOM)

"Diffuse optical mammography" (DOM) is the application of diffuse optical methods to image ("tomography") or to monitor ("spectroscopy") breast cancer physiology [12], [15], [83], [84]. Its history can be traced back to 1920s [85] where non-quantified, primitive diffuse optical measurements were conducted by placing a light source under the breast in order to explore the nature of various lumps that were palpable. Over time, both the technology and the physical models have evolved immensely and DOM is moving steadily towards being a quantitative and robust modality.

Since the late 80s, when the use of the photon diffusion model gained a general acceptance, the clinical feasibility of quantitative DOM has been demonstrated in various breast cancer related applications:

1. The quantification of healthy subject tissue properties [86]–[94] and its correlation with cancer risk prediction [95]–[98].
2. The tumor characterization based on the endogenous contrast [12], [99], [100].
3. The tumor characterization using the exogenous contrast agents based on absorption [101], [102] or fluorescence enhancement [103]–[106].
4. The therapy monitoring by characterization of the changes in the tumor physiology in response to various therapies [44], [82], [107]–[118], and due to tissue healing after laser treatment for fibroadenoma [119] or core biopsy [120].
5. The tracking of the sentinel lymph nodes using fluorescent contrast agents during surgery [121], [122]. (Note that works in these intraoperative references did not employ diffusion model-based quantification.)

Despite these promising advances, the technology is not yet approved for widespread clinical use, but it is steadily progressing towards that goal [15]. There are still great variations in instrumentation and analysis algorithms which reflect the abundance of open research questions and developments. In general, the instrumentation differs with respect to the probe design (e.g., hand-held vs fixed-scanning vs fixed-static), the measurement geometry (e.g., reflectance vs ring vs cone vs parallel-plate), source types (further elaborated in the following Sections), the number and range of wavelengths, the choice of the optode coupling (e.g. fiber-coupled vs free-space), and the number of source/detector pairs. The analysis algorithms range in complexity from basic analytic solutions in simple measurement geometries to nonlinear, iterative, 3D tomo-graphic reconstructions, to region-based reconstructions based on *a priori* spatial information provided by other imaging modalities such as MRI [57], [58], ultrasound [59]–[61], or X-ray tomosynthesis [62], [63].

Regardless of the technical differences, hemodynamic and other physiological properties accessible by the diffuse optical methods are sensitive to physiological variations such as those of the breast tumors as compared to the normal tissues (in space) and to variations in time as the tumor evolves (e.g. growth, angiogenesis, hypoxia) either naturally or in response to cancer therapies. For example, a robust and significant tumor-to-normal contrast of *THC* was reported by most of research groups [12], [99], [100], [123]–[131]. Its origin is attributed to the angiogenesis in the tumor volume. This macroscopically and non-invasively estimated, local total hemoglobin concentration was shown to be correlated with the microscopic histological analysis of the vasculature [113], [132], [133] and particularly with angiogenesis [44]. Furthermore, recently, diffuse correlation spectroscopy (DCS, further elaborated in the following sections) allowed for the measurement of a *microvascular* blood-flow index (*BF*) which was found to be higher in malignant tumors compared to normal tissue [80] which may be due to the interplay between angiogenesis, hypermetabolism and intravascular pressure in the tumor. Some groups have also observed increased tissue

scattering in tumors [99] which may be due to the increase in the number density of subcellular organelles (e.g., mitochondria, nucleolus) from increased proliferation. The lipid content was reported to be lower in tumors compared to normal tissues which may be due to the tumor cells pushing out the breast adipose tissue (which is quite abundant in the breast) [130]. The water concentration was also evaluated and was reported to be higher than the normal tissue [112], [130]. This may be related to the increase in cellularity (the number and type of cells). In other words, the proliferation leads to increased number of cells containing higher amount of water than fatty adipose cells. Furthermore, the water content in the extracellular matrix of tumor can be elevated compared to normal tissue due to leaky vasculatures and the lack of lymphatic drainage [134]. A recent report has attempted to evaluate the percentage of bound water to macromolecules to the unbound water, and in that study it was lower in tumors [135]. The possibility of probing the collagen concentrations by expanding the spectral range beyond 1000 nm was also explored [93], [136]. The underlying hypothesis of these works is that the collagen content, which is the major constituent of stroma, may prove to be yet another valuable parameter accessible by diffuse optics for the differentiation of benign and malignant tumors, since the stromal architecture changes are different between benign and malignant tumors. Another endogenous optical parameter which has exhibited tumor to normal contrast is the local refractive index [137], [138].

As must be evident from the above summary, the optical methods are turning out to be promising for the evaluation of a wide-range of breast tissue properties based on the endogenous contrast. Further sensitivities and improved contrast may be available by the use of exogenous contrast agents (or dyes) [139]. Some of these dyes are not particularly engineered to be specific to the tumor, but still exploit the increased leakiness and/or the vascularity of the tumors to increase the tumor contrast. Other dyes can target tumor by bioconjugation aimed at certain receptors or molecules, and even be utilized to gain information about biochemical properties such as the local pH levels.

For example, indocyanine Green (ICG), the most commonly utilized FDA-approved compound suitable for DOT, has both an absorption and fluorescence spectra in the near-infrared window making it very attractive for DOT/DOS. Based on the fact that the tumors have leakier vasculature, in an analogous fashion to gadolinium enhanced MRI, ICG was utilized to enhance the *absorption* contrast of the human breast cancer *in vivo* [101], [102]. These early studies demonstrated that the ICG enhanced region coregistered well with breast tumor region identified by gadolinium enhancement in MRI [101], and the pharmacokinetics of ICG may provide additional information to differentiate benign and malignant tumors [102]. In principle, the fluorescence of ICG could further improve the detection sensitivity since the background tissue (after complete wash-out of ICG in the normal vasculature) would not have any detectable fluorescence in these wavelengths. In their work, the Sevick-Muraca group studied *fluorescence* DOT imaging using ICG and have demonstrated that the ICG fluorescence signal is detectable in canine breast cancer [140] and reconstructed fluorophore concentration in realistic breast phantoms [141]. As a side note, a significant progress in three-dimensional fluorescence tomography has been achieved in small animal imaging area [142] and was translated to 3D clinical fluorescence DOT of *in vivo* human breast by our group [103] and others [106] demonstrating high ICG accumulation in malignant tumors, presumably due to local angiogenesis and the local leaky vasculature. In particular, a distinction between benign and malignant tumors was demonstrated using 2D absorption-corrected fluorescence projection image taken at 25 minutes after ICG infusion, reflecting microvascular permeability dependency on malignancy [104], [105]. It is expected that with better markers, possibly with targeted ones, the fluorescence signals will provide greater detection sensitivity and specificity compared to the absorption signals, as well as access to new information about tissue micro-environment, such as pO_2, pH, and intracellular calcium concentration [143], [144].

The possibilities do not end here and recently more complex approaches that utilize the generation of ultrasound by light absorption ("photo-acoustics") [145]–[147] , the tagging of light by ultrasound ("acousto-optics") [145], [146] and others based on diffuse optics were introduced. A whole generation of new contrast agents based on nano-particles and light-activated compounds are also emerging and are slowly being translated to pilot clinical tests [148]. Our goal in this section was to provide the readers with the general flavor of "diffuse optical mammography" and a set of references for further details. It is beyond the scope of this paper to cover the whole field of DOM in detail.

IV. Breast cancer therapy monitoring with diffuse optical spectroscopy and imaging (DOS/DOT)

To date, the majority of publications in diffuse optical mammography have either showcased a few case studies or just demonstrated feasibility to distinguish responders from non-responders of neoadjuvant chemotherapy based on the endogenous contrast with a few measurements [13]. In this section, we discuss the characteristics of DOM systems used in the therapy monitoring applications, then present examples of DOT, DOS and DCS for neoadjuvant chemotherapy and targeted therapy monitoring. Several studies demonstrating the feasibility of diffuse optics to predict therapy response are discussed.

A. Characteristics of DOM systems as applied for therapy monitoring

We now highlight main DOM systems that were utilized for published studies on neoadjuvant chemotherapy monitoring. The characteristics of the main systems that were developed and utilized for neoadjuvant chemotherapy monitoring are summarized in Table I. Here we distinguish hand-held DOS (DCS) systems (DOS-1, DCS-2) from stand-alone DOT (DOT-3,4,5) and multi-modal DOT systems (US/DOT-6). The list is, perhaps, not exhaustive and we apologize for any unintended omissions.

Hand-held systems [14] have, due to their relative simplicity and size, a high potential for translation into routine use at a clinician's office. Most importantly, they can access the breast axillary (i.e., underarm) regions much better than the other systems. However, the spatial information available to hand-held systems is limited due to the most often employed reflectance geometry (Figure 2) and the time constraints due to the manual scanning over the breast. This may lead to some inaccuracies in the separation of the signals of the tumor tissue from those of the surrounding healthy tissue. This is also a concern because of problems associated with partial volume effects that may lead to a dependence of the results on the tumor depth and size which can be accounted for by the inclusion of *a priori* knowledge [60].

Stand-alone DOT systems, on the other hand, require more complex instrumentation and dedicated optomechanical components to host the patient. Their advantage lies in the fact that a pre-determined, large set of source-detector pairs could be utilized, and if DOT reconstruction is successful, it could overcome the limitations of hand-held DOS systems and provide an accurate assessment of the tumor physiology and volume (albeit with low spatial resolution).

Multi-modal DOT approach allows one to reconstruct optical properties in 3D regions with less number of source and detector positions than the stand-alone approach, and even when a large number is utilized, it is expected to improve the quantification. The idea is based on the relative ease of combining DOM with other modalities such as X-Ray, Ultrasound and MRI imaging by use of compatible fiber-optics [57]–[62], [94], [100], [101], [149]. This secondary data, taken simultaneously, allows the researchers to segment the tissues and either reconstruct or fit by utilizing this additional information.

In general, in both stand-alone and multi-modal DOT systems, the number of parameters that are reconstructed is less than those of a hand-held DOS system due to the compromise to increase the number of optodes to obtain higher spatial information over spectral information. This limitation is being addressed by some groups by utilizing further hybridization or by the incorporation of broadband sources into DOT systems [93], [150], [151].

In the following, we briefly describe salient features of each system listed in Table I. The system designation (e.g., DOT-5) will be used throughout the paper, especially in the following tables.

1) UCI hand-held system, DOS-1—A hand-held device from the University of California, Irvine (UCI) group (PI: Bruce J. Tromberg) focuses in maximizing the spectral information available in a single source-detector pair by combining a frequency-domain system with sweeping frequencies over wide range and a continuous-wave broadband spectrometer system. This combination enables the group to quantify not only *Hb, HbO_2* and scattering information, but also water, lipid content [152], and the binding state of water to other macromolecules [135].

2) UPENN hand-held system, DCS-2—Another type of hand-held device is from the University of Pennsylvania (UPENN) group (PI: Arjun G. Yodh) based on DCS which provides an entirely new parameter, microvascular blood flow which can readily be combined with DOS [80]. Since DCS is a relatively new technique that has been implemented in a handful of centers, the instrumentation is quite similar amongst different research groups [79], [80], [153]–[158]. Here, one of the instruments used for chemotherapy monitoring [82] is outlined.

As the light source, a continuous-wave, long coherence laser (Crysta Laser, Reno, Nevada) at 785 nm was delivered onto the tissue surface via an optical fiber. The light that has diffused through the breast tissue was collected by four single-mode fibers that were attached to four fast photon-counting avalanche photodiodes (Perkin-Elmer, Quebec, Canada) to detect the intensity fluctuations of the diffusing light in the reflectance geometry. The detectors sent out TTL signals corresponding to each detected photon which was fed to a four-channel custom correlator board (Correlator.com, Bridgewater, New Jersey), and the resulting temporal intensity autocorrelation functions were recorded by a computer. Each full-set of data was acquired every two seconds and five such sets were averaged at each position. For this study, source and detector fibers were separated by 2.5 cm. The resultant auto-correlation functions were then fitted to a solution of the correlation diffusion equation to derive *BF*. These instruments could readily be combined with DOS or DOT systems in either continuous-wave, frequency-domain or time-resolved implementations [16]. For more system details, see [159], [160].

3) UPENN stand-alone DOT system, DOT-3—The CCD-based detection system developed by UPENN group provides a large amount of off-axis measurements that are necessary for full 3D reconstruction. This hybrid system acquires CCD-based CW transmission and fiber-based FD (70MHz modulation) re-emission data from six laser sources with wavelengths spanning from 650 to 905 nm. A major concern for this device is that the majority of data is in CW leading to potential non-uniqueness problems, but the UPENN group has succeeded in the development of 3D nonlinear reconstruction scheme based on a multi-spectral imaging approach [161], [162] and an initial guess estimation using frequency-domain information [99].

4) ART stand-alone DOT system, DOT-4—The design focus of the SoftScan by Advanced Research Technologies Inc. (ART, Montreal, Canada) [125] is different from UPENN system, in that the detection is based on time-domain approach with tandem scanning. This design is an adaption of earlier approaches by other groups [127], [163]–[169]. Generally speaking, tandem scanning employs one source placed in one plane and one detector in the parallel plane, forming only one on-axis measurement pair (Figure 1b, middle row, left panel). Even though it is possible to acquire finely sampled spatial information (e.g., 1-2 mm interval), the lack of off-axis measurements severely limits the possibility of a full 3D reconstruction. However, this potential disadvantage has been overcome by use of four detectors placed around the center detector to enable off-axis measurements [106], [125], [170]. The time domain method has the advantage of providing a high information content per source-detector pair.

5) Dartmouth stand-alone DOT system, DOT-5—The stand-alone DOT system developed by Dartmouth College (PI: Brian W. Pogue) has three rings of fiber arrays [171]. A ring has 16 radial positions, and each position is occupied by one source fiber and one detector fiber. Sequential source multiplexing yields 16 × 15 source-detector pairs per ring. Six laser diodes in 660-850 nm range are modulated at 100 MHz and detected with photomultipliers connected to heterodyne electronics. The image reconstruction is based on finite-element-method forward model and Newton's method [172], [173]. Even though the data do not contain off-plane information, Dartmouth group has shown 3D reconstruction in this geometry is possible and quantitative [171].

While the most of chemotherapy monitoring results introduced in this paper were obtained with the stand-alone system, the Dartmouth group has been performing measurements on breast cancer patients with a concurrent MRI/DOT system in an MRI-bed-based platform [58], [149]. A pilot study of this MRI/DOT system applied to therapy monitoring was presented in a conference [174].

6) UConn multi-modal system, US/DOT-6—Instruments developed by the University of Connecticut group (PI: Quing Zhu) utilize a hand-held type probe combining a 2D ultrasound transducer and a set of optical fibers [61]. Therapy monitoring studies were performed with two prototypes [113]. The first prototype consisted of 780 and 830 nm lasers, 6 source positions and 8 detector positions. The second prototype had 690, 780 and 830 nm lasers, 9 source positions and 10 detector positions. Spatial information from the ultrasound image is incorporated into the DOT reconstruction as *a priori* knowledge through dual-mesh approach where finer mesh is used for tumor region than the rest of the breast.

B. Selected Examples of Therapy Monitoring with Diffuse Optics

In this section, we highlight several studies on breast cancer therapy monitoring to illustrate the concepts that we have been discussing. First, we present a case where a stand-alone DOT and a hand-held DCS were utilized to follow changes in hemodynamic parameters on the same patient. Then an example of chemotherapy response classification using a hand-held multi-modal DOT system is presented. The possibility of using DCS to study blood flow responses induced by new type of therapies follows. These studies were performed at a relatively long time scale (e.g., 2 weeks - 8 weeks after initial therapy). The potential of utilizing multiple hemodynamic parameters including blood flow to differentiate response group early (e.g., a few days after initial therapy) is presented. Then the case study results from several groups are summarized.

1) A case of chemotherapy monitoring using DOT and DCS on a complete responder—A 53-year-old premenopausal female with locally advanced breast cancer was

measured with stand-alone DOT (DOT-3 [99]), hand-held DCS (DCS-2 [82]) and dynamic-contrast enhanced MRI (DCE-MRI) on the same day, at several time points during the neoadjuvant chemotherapy regimen. An ultrasound-guided core biopsy revealed a high grade poorly differentiated invasive ductal carcinoma with negative ER, PR and positive HER2. The therapy consisted of four *AC* cycles (a combination of doxorubicin with Adriamycin as a brand name and Cyclophosphamide; denoted as *AC* treatment here-on) followed by four Taxol cycles at two week intervals. After the completion of chemotherapy, the patient went through a partial mastectomy of the right breast and a right axillary dissection. The pathology analysis revealed no residual carcinoma in the mastectomy specimen and in lymph nodes (i.e., complete pathologic response). This patient was characterized as a complete pathologic responder (pCR) according to our classification scheme described in Section II. However, chronic inflammation and focally calcified dense fibrosis were noted in the mastectomy specimen.

The DOT, DCS, DCE-MRI measurements were performed at three time points; before chemotherapy (pretherapy), between the completion of *AC* therapy and the initiation of Taxol therapy (midtherapy), and at the completion of Taxol therapy, but prior to the surgery (posttherapy). A representative tumor slice from 3D MR images (in sagittal and axial orientations), and from 3D reconstructed total hemoglobin concentration (*THC*) images (in axial orientation) are shown in Figure 4a arranged in the order of pre-, mid-, and post-therapy time point (top, middle, and bottom). The longest tumor dimension measured by DCE-MRI was 4.7 cm at pretherapy and 3.5 cm at midtherapy time point with decreased enhancement, in the lateral position. We note that, in addition to the pathology, a complete imaging response was determined by DCE-MRI at the posttherapy time point.

In the DOT images, a localized high *THC* region was clearly seen at the same position as the MR enhanced region (see axial slices) prior to initiation of therapy. However, at mid- and post-therapy time points, *THC* distribution was more homogeneous across the whole breast. Note, the *THC* colorbar scale was maintained to be at maximum = 2 × minimum while their values change at each time point, since the global *THC* value is susceptible to hematocrit level fluctuations induced by chemotherapy and Neulasta shots. The localized changes of these physiological parameters over time clearly demonstrate the dynamic imaging capability of the DOT method.

The hand-held DCS results are shown in Figure 4b, where the relative blood flow index (*rBF*) normalized to the pretherapy tumor *BF* value shows a gradual decrease with the therapy progression, with a ~50% reduction in blood flow at the end of the therapy. This is in-line with reductions of the contrast uptake by MRI and *THC* reductions by DOT.

2) An example of response classification with multi-modal DOT—As an example of chemotherapy response classification, a hand-held US/DOT-6 system is featured in Figure 5. Three-dimensional DOT images in coronal slice are of 9×9 cm area, and spans from 0.2 cm to 3.2 cm deep from the breast tissue surface. In this figure, a representative DOT slice going through the tumor center was selected and placed side-by-side with corresponding ultrasound at pre-therapy, the end of cycle 2, and post-therapy time points. Note the ultrasound is in sagittal orientation, but DOT slice is in coronal orientation. Image sets in the left and right show images from a responder and a non-responder respectively. The responder (66 year-old) had 1.8 × 2.0 × 3.7 cm size tumor with high grade invasive ductal carcinoma initially, but achieved complete pathologic response (pCR) at the end of chemotherapy. Blood volume index (BVI = tumor volume × tumor $\overline{THC}$) for this patient decreased around 80% from pre-therapy value. The non-responder (49 year-old) had 3.8 × 2.8 × 2.3 cm tumor with low-grade invasive ductal carcinoma initially, and had 3.3 cm residual tumor at the time of surgery (i.e., pPR4). In this case, no reduction in %BVI was

observed. This trend is clearly seen in the DOT images: the high contrast region in responder show dramatic decrease (Figure 5b left) whereas similar high contrast region persists in the non-responder (Figure 5b right).

3) Blood flow monitoring for neoadjuvant targeted therapy—Molecularly targeted therapies employ drugs that interfere with specific molecules involved in tumor growth and progression. Among many targeted therapies, Lapatinib inhibits both the epidermal growth factor receptor (EGFR) and HER2 tyrosine kinases [176]. We had a unique opportunity to take part in a Phase II exploratory study at UPENN to analyze the molecular determinants of response to Lapatinib, including core-biopsies, DCE-MRI, MRS, and DCS before and after therapy.

A 37 year-old premenopausal female was measured with DCS and DCE-MRI before and after 14 days of daily oral administration of Lapatinib as a monotherapy (phase II clinical trial). The tumor size measured by the ultrasound was 2.6 × 1.4 × 2.0 cm. A core biopsy analysis showed high-grade invasive ductal carcinoma. The surgical pathology after the completion of Lapatinib revealed a poorly differentiated high grade (mBR = 8) invasive ductal carcinoma in 2.5 cm region. MRI did not show any size changes between pre- and post-time points (2.8 × 2.3 cm).

As shown in Figure 6, DCS observed a significant BF change, which may be due to the re-normalization effect of Lapatinib. In an earlier animal study, we have shown that EGFR inhibitors normalize the tumor vasculature by decreasing HIF-1α and VEGF [177] where a similar response was observed by DCS on murine tumors. The decrease of these factors results in a decrease of vessel permeability and an increase of blood flow. At this point, it is unclear whether the observed blood flow increase was due to the re-normalization effect of Lapatinib or due to the tumor progression, since we did not have a more comprehensive set of hemodynamic parameters and a microscopic validation. Regardless, this example demonstrates that DCS/DOS can readily be incorporated into new clinical trials to study the hemodynamic effects of new targeted therapies in humans.

4) An example of response classification based on early hemodynamic biomarkers—In the previous example of a complete responder (Section IV-B1), the disappearance of the high tumor-to-normal contrast THC region in a 3D map, and the decrease of the tumor blood flow were expected based on anti-vascular effects of successful therapy. These data are interesting but depicts results at the midtherapy time point when the first regimen is completed (i.e., eight weeks after the initial therapy in this particular case), which may be too late for intervention. For optimal treatment optimization (e.g., changing treatment regimen for nonresponders), the monitoring method needs to provide response prediction at early time point (e.g., days or a few weeks after initial treatment).

In a pilot study to investigate the possibility for early therapy response prediction, we have measured two subjects undergoing neoadjuvant chemotherapy every one to two days up to ten days after the initial therapy. One subject was a 45-year-old premenopausal female with an invasive ductal carcinoma spanning 8.5 × 5 cm area as measured by MRI before the therapy. The subject went through four cycles of AC and seven cycles of Taxane treatment. A lumpectomy after the completion of chemotherapy revealed a moderately differentiated residual invasive ductal carcinoma in a 0.5 cm region with extensive fibrosis. This response corresponds to pPR1 (i.e., good response). Note that this data was acquired as a collaborative project between UPENN and UCI groups and published in [82] as a case study. The other subject was a 55-year-old premenopausal female with a biopsy-proven lesion of 8.5 × 5.8 cm size measured by MRI. The subject went through four cycles of Taxane, followed by four cycles of AC. Even at the completion of the chemotherapy, a 6 cm

invasive lobular carcinoma was found in the mastectomy sample. This response corresponds to pPR3 (i.e., poor response).

Figure 7 shows $rBF = BF/BF_{pre}$ (left column) and $rTHC = THC/THC_{pre}$ (right column) changes in the tumor region. In the good response case, pPR1, (top), there was a transient increase in BF followed by a gradual decrease, whereas $rTHC$ decreased significantly at day four and stayed at that level. On the other hand, when the response was poor, pPR3, (bottom), rBF gradually increased and $rTHC$ had an increasing trend throughout the therapy. This anecdotal evidence demonstrates that it may be possible to discriminate between good and poor responders based on the early hemodynamic response and different biomarkers may provide different information.

5) Summary of case studies—Several case studies summarized in Table II have demonstrated (1) the trend of changes in optically measurable parameters due to chemotherapy are as expected for given tumor response [82], [107]–[111], [116], (2) the tumor volume estimated with optical parameters follow similar trends as the tumor volume changes measured with DCE-MRI [108], [109], and (3) the use of multiple optical parameters may allow diffuse optics to be sensitive to early changes due to chemotherapy [82], [107], [110], [116].

Most of case studies outlined in Table II were performed on cancer patients undergoing AC treatments. Sometimes multiple AC cycles were followed by multiple cycles of Taxane: paclitaxel (brand name: Taxol) or docetaxel (brand name: Taxotere). This sequence of treatment is called $AC \rightarrow T$ regimen. Most of DOM measurements have characterized only the response to AC treatment (especially daily monitoring studies), whereas long-term measurements (e.g., post-therapy time point) included cumulative effects of AC and T cycles [108], [109]. Notably, a frequent monitoring case study [116] featured another type of targeted therapy, anti-angiogenic Bevacizumab (trade name: Avastin).

According to our pathologic classification criteria based on the tumor size, patients in most of case studies have achieved partial responses of varying degree: except one case of pCR3, most cases achieved more than 50% tumor reduction which are generally thought as a favorable outcome. UCI group observed a decrease in THC and water, and an increase in the lipid content in most cases [107], [109], which corresponds to a decrease in the tissue optical index ($TOI = \frac{THC \times H_2O}{\%lipid}$) [110], [116]. While other DOT systems have limitations in the number of accessible parameters, a THC decrease has been consistently observed by others as well [108], [111].

While these examples are interesting and may have clinical implications, data from more patients belonging either in responding or non-responding groups are necessary to determine whether any parameters measured with diffuse optics can distinguish between these response groups reliably. This is the best step towards building a therapy prediction model.

C. Therapy Prediction with Diffuse Optics

In order to predict the therapy response, one needs to identify the best parameters and the optimal time points that provide a significant distinction between responding and non-responding groups (however they may be defined). Several research groups have conducted studies to address these issues, as summarized in Table III. Unlike case studies presented in earlier sections where AC or $AC \rightarrow T$ regimens were dominant, most of these studies included patients under different types of treatment regimens, except AC only evaluation in reference [112]. Some of this variation involve different types of cytotoxic treatment other than $AC \rightarrow T$ or additional treatment using Trastuzumab or Bevacizumab. Even though there

are wide variations in the chemotherapy, the hemodynamic responses seem to be dictated mainly by different degree of pathologic response, and not by the therapy types according to a statistical analysis [117]. Still, the response characteristics of new therapies may not be so universal, considering that their targeting mechanism involves different biological pathways and time scale from conventional chemotherapy. In addition to therapy type, there are variations in the response classification and the measurement time points in each study. Many studies employed binary classification (i.e., responding vs non-responding group) with the following variations: pCR vs non-pCR, or good (pCR + pPR1,2) vs poor (pPR3,4) response. Even when the studies employed tertiary classification, statistical analysis still yielded mostly binary results [117], [118]. Therefore, the response groups in the Table III are presented in such a way to highlight the major results of each study using binary grouping. In terms of measurement time, most studies span pre- to post-therapy time period, except some studies focusing on early responses [112], [117].

There are interesting trends in Table III. The measurable parameters that are good predictors of the therapy response and the earliest time point where a classification of the different response (i.e., the optimal time) is observed have some systematic trends. The predictor parameters at early time points (1 day or 1 week after the initial therapy) distinguished good vs poor responding groups [112], [117], whereas at the late time points (mid- or post-therapy) they distinguished pCR vs non-pCR groups [44], [118]. If this trend holds true, then its potential impact in the treatment optimization can be significant. At the early stage of the treatment, it is important to figure out who will not benefit from this particular treatment, so that the treatment can be changed and the patient can be spared of the unnecessary side-effects. At the completion of each treatment regimen, knowing who will not achieve pCR may guide the decision whether to continue with neoadjuvant therapy before moving onto surgery.

Here, let us look at the therapy predictors with respect to optimal time point in detail. The earliest time points exhibiting a significant difference between various group of patients were different among the studies cited. The time points can be roughly divided into early, four weeks after the initial therapy, mid-therapy (i.e., after completion of the first regimen and before start of the second regimen), and the post-therapy time points. Due to wide variations in the available measurement time points, a direct comparison among studies is difficult. In terms of the parameters identified as predictors, all of them except the early HbO_2 flare [117] showed a statistically significant *decrease* in the responding group when compared to the non-responding group.

In Roblyer *et al* paper [117] (Figure 8), where the early HbO_2 flare is emphasized, one day after the initial therapy, the HbO_2 concentration *increased* significantly in the good responding group (i.e., pCR and pPR1,2), whereas HbO_2 decreased in the poor responding group (i.e., pPR3,4). Figure 8 also shows, while statistically non-significant, trends of *increases* in all other parameters in the pCR group as compared to the other groups. These findings are generally in-line with the above-mentioned trends.

Cerussi *et al* [112] specifically explored the hemodynamic and tissue physiological responses one week after the initial *AC* therapy and found a decrease in *Hb,* HbO_2 and relative water after 1 week was much larger for responders compared with non-responders. On the other hand, Soliman *et al* [115] measured at prior to, one, four and eight weeks after the initial treatment time points, and found that the four week after time point yielded a statistically significantly different distinction between the response groups compared to the one week time point. This discrepancy may be due to the differences in the classification of the response group and the chemotherapy regimen. Cerussi *et al* had patients with pCR, pPR1 and pPR2 in the responding group, whereas Soliman *et al* had only patients with

pPR2. Also, all the patients in the study of Cerussi *et al* had *AC* treatments, whereas ten patients in the study of Soliman *et al* had six different therapy regimens. Note that only the data from the eight patients were categorized into different response groups in Table III, due to complicated responses in two cases. One of these cases is particularly interesting; the treatment plan was changed when the axillary node size was increasing with time even with the initiation of treatment. Diffuse opticsl measurements showed an *increase* in all the parameters after the first treatment, then a significant *decrease* after the change of the regimen to a more effective treatment plan. This anecdotal data indicates that the changes detected by diffuse optics follow the treatment effectiveness (assessed by morphological means) closely. This characteristics may someday lead diffuse optics to become a complementary tool for therapy guidance.

Four weeks after the initial therapy time point was explored by several groups [113]–[115]. They found that the decrease in *THC* or a *THC*-related parameter to be a robust predictor. Looking further at even later time points, either *THC* or *TOI* turned out to be reliable predictors [44], [118].

Overall, these studies have demonstrated the potential role of the hemodynamic parameters in the prediction of the therapy response. Furthermore, the sensitivity of the microvascular, local blood flow to the response was showcased in this paper as an anecdotal data. This dynamic blood flow information, accessible by DCS, combined with DOS may, for example, confirm the HbO_2 flare phenomena and/or offer a finer classification of the prediction at an early stage. It may also have a role in developing, characterizing and monitoring targeted therapies. In addition, groups with the capabilities to probe the water content reported this parameter to be a strong predictor [112], or a near-significant predictor [115]. Lipid information which enters into the tissue optical index *TOI* seems to be a good predictor at the late time points. Clearly, there is still a lot to be explored with diffuse optics.

Understanding the physiological origin of the optical signals with respect to the therapy prediction is also important for validation and further development. As an example, an investigation comparing *THC* with CD31 (vasculature marker) and CD105 (neovasculature marker) revealed that the *THC* change before and after chemotherapy correlated well with changes in the measured neovasculature marker. This implies that the *THC* changes are, indeed, sensitive to the changes in tumor angiogenesis [44].

V. Conclusions

While these results are promising, these studies have serious limitations in terms of patient statistics. Most of the earlier prediction studies had seven to eleven patients which were further divided into two or three response groups. This is further hampered by different definitions of responding and non-responding groups employed by each group. To fully explore the role of diffuse optics in therapy monitoring, a significant number of new patient data is needed.

Recent additions to the literature report cohorts of more than twenty patients [117], [118] which is a step in the right direction. A multi-center clinical trial by the American College of Radiology Imaging Network (ACRIN 6691, PI: Tromberg) has just been launched in the year 2011. A standardized instrument and data analysis (DOS-1 system, described in Table I) will be utilized to measure patients in five participating research centers spread across North America. The optical measurements will be performed at the baseline, early therapy (e.g., 1 week after initial chemotherapy), mid-therapy (i.e., before the start of the second therapy regimen; ~ 8-12 weeks), and post-therapy time points (~ 16-24 weeks). The breast coverage has been extended from a line-scan [107], [112] to a 2D grid to enable a 2D

topographic representation of data [117], [118]. The primary aim is to determine whether baseline to mid-therapy changes in optical measurements can predict pathological response in patients. The secondary aims are to investigate the early prediction capability and the correlation with MRI. We believe that with this trial and other future multi-center trials, the field will achieve the much needed maturity.

So far, we have reviewed the progress in the clinical therapy monitoring based on the endogenous parameters. To our knowledge, fluorescence diffuse optical tomography (FDOT) based on the exogenous contrast agent injection has just started and yet to demonstrate its usefulness in the clinical therapy monitoring [174]. This is partly due to the limited availability of FDA-approved fluorescent contrast agents. In the future, FDOT coupled with novel molecularly targeted fluorescent dyes may offer a different spectrum of information such as the direct visualization of the drug uptake in the tumor or targeted therapy effect sensors [4] in addition to the endogenous information. These collective information can contribute greatly towards new therapy developments.

As the number of parameters increases, it will be important to develop computer-aided, statistical classification/prediction models similar to those reported for classification of the DOT images [178]. These approaches may help to combine the wealth of information available from the diffuse optical data and the other modalities in a systematic way.

Acknowledgments

The authors acknowledge grant support from NIH-grants CA-126187, EB-02109, RR-02305, and Fundació Cellex Barcelona, Marie Curie IRG (RPTAMON, FP7), Instituto de Salud Carlos III (FIS), Ministerio de Ciencia e Innovación, Spain (MICINN) and Photonics4Life (FP7). We are most grateful to Arjun G. Yodh at the University of Pennsylvania who has been an advisor and a mentor for both of us for many years and in whose lab most of the studies mentioned in this paper were conducted at. The authors also thank current and past members of the Yodh laboratory at the University of Pennsylvania for discussions and interactions over the years. We thank David R. Busch and Yoo Kyung Choe, in particular, for providing some of the figures.

Much of the original research illustrated in this review was facilitated by collaborations over many years with Mitchell D. Schnall, Angela DeMichele, Mark A. Rosen, Rebecca Davidson, Brian J. Czerniecki, Douglas L. Fraker, Julia Tchou, Carolyn Mies, Michael Feldman, Luke Velders, Britton Chance at the University of Pennsylvania, and Bruce J. Tromberg, Albert Cerussi at the University of California, Irvine.

Biography

Regine Choe received her B.S. in physics from the Pohang University of Science & Technology, Korea in 1996, and Ph.D. degree in physics from the University of Pennsylvania, in 2005. After finishing her postdoctoral work at the University of Pennsylvania, she joined the Biomedical Engineering department of the University of Rochester as an Assistant Professor, in 2011. Her research is focused on the development of diffuse optical methods for the clinical application of breast cancer diagnosis and therapy monitoring.

Turgut Durduran received his B.A. and Ph.D. in physics at the University of Pennsylvania, in 1997 and 2004 respectively. After completion of his research work at the University of Pennsylvania, he moved to ICFO-The Institute of Photonic Sciences in Barcelona, Spain to start the "Medical Optics" group in 2009. His main research interest is in the development of diffuse optical technologies for clinical applications.

References

1. [Sep. 1, 2011] American cancer society, global cancer facts & figures 2nd edition. http://www.cancer.org/Research/CancerFactsFigures/GlobalCancerFactsFigures/global-facts-figures-2nd-ed
2. [Sep. 1, 2011] American cancer society, cancer facts & figures 2011. http://www.cancer.org/Research/CancerFactsFigures/CancerFactsFigures/cancer-facts-figures-2011
3. [Sep. 1, 2011] National comprehensive cancer network clinical practice guidelines in oncology, version 2.2011. http://www.nccn.com
4. de Vries EGE, Munnink THO, van Vugt MATM, Nagengast WB. Toward molecular imaging-driven drug development in oncology. Cancer Discovery. 2011:25–28. [PubMed: 22586317]
5. Barker AD, Sigman CC, Kelloff GJ, Hylton NM, Berry DA, Esserman LJ. I-SPY2: an adaptive breast cancer trial design in the setting of neoadjuvant chemotherapy. Clinical Pharmacology & Therapeutics. 2009; 86:97–100. [PubMed: 19440188]
6. Schwartz GF, Birchansky CA, Komarnicky LT, Mansfield CM, Cantor RI, Biermann WA, Fellin FM, McFarlane J. Induction chemotherapy followed by breast conservation for locally advanced carcinoma of the breast. Cancer. 1994; 73:362–369. [PubMed: 8293401]
7. Sledge GW. Preoperative chemotherapy for breast cancer: Lessons learned and future prospects. J. Clin. Oncol. 2003; 21(24):4481–4482. [PubMed: 14625269]
8. Fisher B, Bryant J, Wolmark N, Mamounas E, Brown A, Fisher ER, Wickerham DL, Begovic M, DeCillis A, Robidoux A, Margolese RG, Cruz AB Jr, Hoehn JL, Lees AW, Dimitrov NV, Bear HD. Effect of preoperative chemotherapy on the outcome of women with operable breast cancer. J. Clin. Oncol. 1998; 16(8):2672–2685. [PubMed: 9704717]
9. van der Hage JA, van de Velde CJH, Julien J-P, Tubiana-Hulin M, Vandervelden C, Duchateau L. Pre-operative chemotherapy in primary breast cancer: Results from the European Organization for Research and Treatment of Cancer Trial 10902. J. Clin. Oncol. 2001; 19:4224–4237. [PubMed: 11709566]
10. Rastogi P, Anderson SJ, Bear HD, Geyer CE, Kahlenberg MS, Robidoux A, Margolese RG, Hoehn JL, Vogel VG, Dakhil SR, Tamkus D, King KM, Pajon ER, Wright MJ, Robert J, Paik S, Mamounas EP, Wolmark N. Preoperative chemotherapy: updates of National Surgical Adjuvant Breast and Bowel Project Protocols B-18 and B-27. J. Clin. Onc. 2008; 26:778–785.
11. Caudle AS, Gonzalez-Angulo AM, Hunt KK, Liu P, Pusztai L, Symmans WF, Kuerer HM, Mittendorf EA, Hortobagyi GN, Meric-Bernstam F. Predictors of tumor progression during neoadjuvant chemotherapy in breast cancer. J. Clin. Onc. 2010; 28:1821–1828.
12. Leff DR, Warren OJ, Enfield LC, Gibson A, Athanasiou T, Patten DK, Hebden J, Yang GZ, Darzi A. Diffuse optical imaging of the healthy and diseased breast: A systematic review. Breast Cancer Res. Treat. 2008; 108:9–22. [PubMed: 17468951]
13. Enfield LC, Gibson AP, Hebden JC, Douek M. Optical tomography of breast cancer - monitoring response to primary medical therapy. Targ. Oncol. 2009; 4:219–233.

14. Erickson SJ, Godavarty A. Hand-held based near-infrared optical imaging devices: a review. Med. Eng. Phys. 2009; 31:495–509. [PubMed: 19054704]
15. Tromberg BJ, Pogue BW, Paulsen KD, Yodh AG, Boas DA, Cerussi AE. Assessing the future of diffuse optical imaging technologies for breast cancer management. Med. Phys. 2008; 35:2443–2451. [PubMed: 18649477]
16. Durduran T, Choe R, Baker WB, Yodh AG. Diffuse optical spectroscopy and tomography for tissue monitoring and imaging. Rep. Prog. Phys. 2010; 73:076701.
17. Elmore JG, Armstrong K, Lehman CD, Fletcher SW. Screening for breast cancer. JAMA. 2005; 293:1245–1256. [PubMed: 15755947]
18. Cocconi G, Di Blasio B, Alberti G, Bisagni G, Botti E, Peracchia G. Problems in evaluating response of primary breast cancer to systemic therapy. Breast Cancer Res. Treat. 1984; 4:309–313. [PubMed: 6549147]
19. Segel MC, Paulus DD, Hortobagyi GN. Advanced primary breast cancer: assessment at mammography of response to induction chemotherapy. Radiology. 1988; 169:49–54. [PubMed: 3420282]
20. Vinnicombe SJ, MacVica AD, Guy RL, Sloane JP, Powles TJ, Knee G, Husband JE. Primary breast cancer: mammographic changes after neoadjuvant chemotherapy, with pathologic correlation. Radiology. 1996; 198:333–340. [PubMed: 8596827]
21. Evelhoch JL, Gillies RJ, Karczmar GS, Koutcher JA, Maxwell RJ, Nalcioglu O, Raghunand N, Ronen SM, Ross BD, Swartz HM. Applications of magnetic resonance in model systems: cancer therapeutics. Neoplasia. 2000; 2:152–165. [PubMed: 10933074]
22. Esserman L, Hylton N, Yassa L, Barclay J, Frankel S, Sickles E. Utility of magnetic resonance imaging in the management of breast cancer: evidence for improved preoperative staging. J. Clin. Oncol. 1999; 17(1):110–119. [PubMed: 10458224]
23. Knopp MV, Brix G, Junkermann HJ, Sinn HP. MR mammography with pharmacokinetic mapping for monitoring of breast cancer treatment during neoadjuvant therapy. Magn. Reson. Imaging Clin. N. Am. 1994; 2(4):633–658. [PubMed: 7489314]
24. Tsuboi N, Ogawa Y, Inomata T, Yoshida D, Yoshida S, Moriki T, Kumon M. Changes in the findings of dynamic MRI by preoperative CAF chemotherapy for patients with breast cancer of stage II and III: pathologic correlation. Oncol. Rep. 1999; 6(4):727–732. [PubMed: 10373646]
25. Drew PJ, Kerin MJ, Mahapatra T, Malone C, Monson JR, Turnbull LW, Fox JN. Evaluation of response to neoadjuvant chemoradiotherapy for locally advanced breast cancer with dynamic contrast-enhanced MRI of the breast. Eur. J. Surg. Oncol. 2001; 27:617–620. [PubMed: 11669587]
26. Yeh E, Slanetz P, Kopans DB, Rafferty E, Georgian-Smith D, Moy L, Halpern E, Moore R, Kuter I, Taghian A. Prospective comparison of mammography, sonography, and MRI in patients undergoing neoadjuvant chemotherapy for palpable breast cancer. Am. J. Roentgenol. 2005; 184:868–877. [PubMed: 15728611]
27. Partridge SC, Gibbs JE, Lu Y, Esserman LJ, Tripathy D, Wolverton DS, Rugo HS, Hwang ES, Ewing CA, Hylton NM. MRI measurements of breast tumor volume predict response to neoadjuvant chemotherapy and recurrence-free survival. Am. J. Roentgenol. 2005; 184:1774–1781. [PubMed: 15908529]
28. Hylton, NM.; Blume, J.; Bernreuter, W.; Pisano, E.; Rosen, M.; Morris, E.; Weatherall, P.; Lehman, C.; Polin, S.; Newstead, G.; Marques, H.; Schnall, M.; Esserman, LJ. Radiological Society of North America Scientific Assembly and Annual Meeting Program. Radiological Society of North America; Oak Brook, Il: 2008. MRI assessment of breast cancer response to neoadjuvant chemotherapy: preliminary findings of the American College of Radiology Imaging Network (ACRIN) trial 6657 [abstract]; p. 267
29. Rosen EL, Eubank WB, Mankoff DA. FDG PET, PET/CT, and breast cancer imaging. RadioGraphics. 2007; 27:S215–S229. [PubMed: 18180228]
30. Wahl RL, Zasadny K, Helvie M, Hutchins GD, Cody R. Metabolic monitoring of breast cancer chemohormonotherapy using positron emission tomography (PET): Initial evaluation. J. Clin. Oncol. 1993; 11:2101–2111. [PubMed: 8229124]
31. Tiling R, Linke R, Untch M, Richter A, Fieber S, Brinkbäumer K, Tatsch K, Hahn K. ^{18}F-FDG PET and ^{99m}Tc-sestamibi scintimammography for monitoring breast cancer response to

neoadjuvant chemotherapy: a comparative study. Eur. J. Nucl. Med. 2001; 28:711–720. [PubMed: 11440031]

32. Quon A, Gambhir SS. FDG-PET and beyond: molecular breast cancer imaging. J. Clin. Oncol. 2005; 23:1664–1673. [PubMed: 15755974]
33. Rousseau C, Devillers A, Sagan C, Ferrer L, Bridji B, Campion L, Ricaud M, Bourbouloux E, Doutriaux I, Clouet M, Berton-Rigaud D, Bouriel C, Delecroix V, Garin E, Rouquette S, Resche I, Kerbrat P, Chatal JF, Campone M. Monitoring of early response to neoadjuvant chemotherapy in stage II and III breast cancer by [^{18}F]Fluorodeoxyglucose positron emission tomography. J. Clin. Onc. 2006; 24:5366–5372.
34. Beresford M, Padhani AR, Goh V, Makris A. Imaging breast cancer response during neoadjuvant systemic therapy. Expert Rev. Anticancer Ther. 2005; 5:893–905. [PubMed: 16221058]
35. McLaughlin R, Hylton N. MRI in breast cancer therapy monitoring. NMR Biomed. 2011; 24:712–720. [PubMed: 21692116]
36. Meisamy S, Bolan PJ, Baker EH, Bliss RL, Gulbahce E, Everson LI, Nelson MT, Emory TH, Tuttle TM, Yee D, Garwood M. Neoadjuvant chemotherapy of locally advanced breast cancer: Predicting response with in vivo ^{1}H MR spectroscopy - A pilot study at 4T. Radiology. 2004; 233:424–431. [PubMed: 15516615]
37. Mankoff DA, Dunnwald LK, Gralow JR, Ellis GK, Schubert EK, Charlop AW, Tseng J, Rinn KJ, Livingston RB. [Tc-99m]-sestamibi uptake and washout in locally advanced breast cancer are correlated with tumor blood flow. Nuclear Med. Biol. 2002; 29:719–727.
38. Dunnwald LK, Gralow JR, Ellis GK, Livingston RB, Linden HM, Lawton TJ, Barlow WE, Schubert EK, Mankoff DA. Residual tumor uptake of [^{99m}Tc]-Sestamibi after neoadjuvant chemotherapy for locally advanced breast carcinoma predicts survival. Cancer. 2005; 103:680–688. [PubMed: 15637688]
39. Debled M, Mauriac L. Neoadjuvant chemotherapy: are we barking up the right tree? Annals of Oncology. 2010; 21:675–679. [PubMed: 20338876]
40. Makris A, Powles TJ, Kakolyris S, Dowsett M, Ashley SE, Harris AL. Cancer. Reduction in angiogenesis after neoadjuvant chemoendocrine therapy in patients with operable breast carcinoma. 1999; 85(9):1996–2000.
41. Feldmann HJ, Molls M, Vaupel P. Blood flow and oxygenation status of human tumors. Strhlentherapie und Onkologie. 1999; 175:1–9.
42. Vaupel P, Hockel M. Blood supply, oxygenation status and metabolic micromilieu of breast cancers: characterization and therapeutic relevance. Int. J. Oncol. 2000; 17(5):869–879. [PubMed: 11029486]
43. Hockel M, Vaupel P. Tumor hypoxia: Definitions and current clinical, biologic, and molecular aspects. J. Natl. Cancer Inst. 2001; 93:266–276. [PubMed: 11181773]
44. Pakalniskis MG, Wells WA, Schwab MC, Froehlich HM, Jiang S, Li Z, Tosteson TD, Poplack SP, Kaufman PA, Pogue BW, Paulsen KD. Tumor angiogenesis change estimated by using diffuse optical spectroscopic tomography: Demonstrated correlation in women undergoing neoadjuvant chemotherapy for invasive breast cancer? Radiology. 2011; 259:365–374. [PubMed: 21406632]
45. Symmans WF, Peintinger F, Hatzis C, Rajan R, Kuerer H, Valero V, Assad L, Poniecka A, Hennessy B, Green M, Buzdar AU, Singletary SE, Hortobagyi GN, Pusztai L. Measurement of residual breast cancer burden to predict survival after neoadjuvant chemotherapy. Journal of Clinical Oncology. 2007; 25:4414–4422. [PubMed: 17785706]
46. Arridge SR. Photon-measurement density functions. Part 1: Analytical forms. Appl. Opt. 1995; 34(31):7395–7409. [PubMed: 21060614]
47. Hebden JC, Arridge SR, Delpy DT. Optical imaging in medicine: I. experimental techniques. Phys. Med. Biol. 1997; 42:825–840. [PubMed: 9172262]
48. Hebden JC, Delpy DT. Diagnostic imaging with light. Br. J. Radiol. 1997; 70:S206–S214. [PubMed: 9534736]
49. Arridge SR, Hebden JC. Optical imaging in medicine: II. Modelling and reconstruction. Phys. Med. Biol. 1997; 42:841–854. [PubMed: 9172263]
50. Villringer A, Chance B. Non-invasive optical spectroscopy and imaging of human brain function. Trends Neurosci. 1997; 20:435–442. [PubMed: 9347608]

51. Ntziachristos V, Chance B. Probing physiology and molecular function using optical imaging: applications to breast cancer. Breast Cancer Res. 2001; 3:41–46. [PubMed: 11250744]
52. Arridge SR, Schotland JC. Optical tomography: forward and inverse problems. Inverse Problems. 2009; 25:123010.
53. Yu, G.; Durduran, T.; Zhou, C.; Cheng, R.; Yodh, AG. Near-infrared diffuse correlation spectroscopy for assessment of tissue blood flow. In: Boas, D.; Pitris, C.; Ramanujam, N., editors. Handbook of Biomedical Optics. CRC Press; Boca Raton: 2011. p. 195-216.
54. Mesquita, RC.; Yodh, AG. Diffuse optics: Fundamentals and tissue applications. In: Kaiser, R.; Weirsma, DS.; Fallini, L., editors. Proceedings of the International School of Physics "Enrico Fermi" Course CLXXIII "Nano Optics and Atomics: Transport of Light and Matter Waves". Vol. 173. 2011. p. 51-74.
55. Gibson AP, Hebden JC, Arridge SR. Recent advances in diffuse optical imaging. Phys. Med. Biol. 2005; 50:R1–R43. [PubMed: 15773619]
56. Pogue BW, Leblond F, Krishnaswamy V, Paulsen KD. Radiologic and near-infrared/optical spectroscopic imaging: Where is the synergy? Am. J. Roentgenol. 2010; 195:321–332. [PubMed: 20651186]
57. Ntziachristos V, Yodh AG, Schnall MD, Chance B. MRI-guided diffuse optical spectroscopy of malignant and benign breast lesions. Neoplasia. 2002; 4:347–354. [PubMed: 12082551]
58. Carpenter CM, Srinivasan S, Pogue BW, Paulsen KD. Methodology development for three-dimensional MR-guided near infrared spectroscopy of breast tumors. Opt. Express. 2008; 16:17 903–17 914.
59. Zhu Q, Durduran T, Ntziachristos V, Holboke M, Yodh AG. Imager that combines near-infrared diffusive light and ultrasound. Opt. Lett. 1999; 24:1050–1052. [PubMed: 18073937]
60. Holboke MJ, Tromberg BJ, Li X, Shah N, Fishkin J, Kidney D, Butler J, Chance B, Yodh AG. Three-dimensional diffuse optical mammography with ultrasound localization in a human subject. J. Biomed. Opt. 2000; 5:237–247. [PubMed: 10938789]
61. Zhu Q, Tannenbaum S, Kurtzman SH. Optical tomography with ultrasound localization for breast cancer diagnosis and treatment monitoring. Surg. Oncol. Clin. N. Am. 2007; 16:307–321. [PubMed: 17560514]
62. Li A, Miller EL, Kilmer ME, Brukilacchio TJ, Chaves T, Stott J, Zhang Q, Wu T, Chorlton M, Moore RH, Kopans DB, Boas DA. Tomographic optical breast imaging guided by three-dimensional mammography. Appl. Opt. 2003; 42:5181–5190. [PubMed: 12962399]
63. Boverman G, Miller EL, Li A, Zhang Q, Chaves T, Brooks DH, Boas DA. Quantitative spectroscopic diffuse optical tomography of the breast guided by imperfect *a priori* structural information. Phys. Med. Biol. 2005; 50:3941–3956. [PubMed: 16177522]
64. Azar FS, Lee K, Khamene A, Choe R, Corlu A, Konecky SD, Sauer F, Yodh AG. Standardized platform for coregistration of non-concurrent diffuse optical and magnetic resonance breast images obtained in different geometries. J. Biomed. Opt. 2007; 12:051902. [PubMed: 17994885]
65. Briers JD. Laser doppler, speckle and related techniques for blood perfusion mapping and imaging. Physiol. Meas. 2001; 22:R35–66. [PubMed: 11761081]
66. Boas DA, Dunn AK. Laser speckle contrast imaging in biomedical optics. J. Biomed. Opt. 2010; 15:011109. [PubMed: 20210435]
67. Bonner, RF.; Nossal, R. Laser-Dopper blood flowmetry. Vol. 107. Kluwer Academic Publishers; Boston: 1990. Principles of Laser-Doppler flowmetry; p. 17-45.
68. Boas DA, Campbell LE, Yodh AG. Scattering and imaging with diffusing temporal field correlations. Phys. Rev. Lett. 1995; 75:1855–1858. [PubMed: 10060408]
69. Boas DA, Yodh AG. Spatially varying dynamical properties of turbid media probed with diffusing temporal light correlation. J. Opt. Soc. Am. A. 1997; 14:192–215.
70. Pine DJ, Weitz DA, Chaikin PM, Herbolzheimer E. Diffusing wave spectroscopy. Phys. Rev. Lett. 1988; 60:1134–1137. [PubMed: 10037950]
71. Maret G, Wolf PE. Multiple light scattering from disordered media. the effect of brownian motion of scatterers. Z. Phys. 1987; 65:409–413.
72. Stephen MJ. Temporal fluctuations in wave propagation in random media. Phys. Rev. B. 1988; 37:1–5.

73. Culver JP, Durduran T, Furuya T, Cheung C, Greenberg JH, Yodh AG. Diffuse optical tomography of cerebral blood flow, oxygenation, and metabolism in rat during focal ischemia. J. Cereb. Blood Flow Metab. 2003; 23:911–924. [PubMed: 12902835]
74. Zhou C, Yu GQ, Furuya D, Greenberg JH, Yodh AG, T D. Diffuse optical correlation tomography of cerebral blood flow during cortical spreading depression in rat brain. Opt. Express. 2006; 14:1125–1144. [PubMed: 19503435]
75. Lemieux PA, Durian DJ. Investigating non-gaussian scattering processes by using nth-order intensity correlation functions. J. Opt. Soc. Am. A. 1999; 16:1651–1664.
76. Irwin D, Dong L, Shang Y, Cheng R, Kudrimoti M, Stevens SD, Yu G. Influences of tissue absorption and scattering on diffuse correlation spectroscopy blood flow measurements. Biomed. Opt. Express. 2011; 2:1969–1985. [PubMed: 21750773]
77. Ninck M, Untenberger M, Gisler T. Diffusing-wave spectroscopy with dynamic contrast variation: disentangling the effects of blood flow and extravascular tissue shearing on signals from deep tissue. Biomed. Opt. Express. 2010; 1:1502–1513. [PubMed: 21258565]
78. Carp SA, Roche-Labarbe N, Franceschini MA, Srinivasan VJ, Sakadžić S, Boas DA. Due to intravascular multiple sequential scattering, diffuse correlation spectroscopy of tissue primarily measures relative red blood cell motion within vessels. Biomed. Opt. Express. 2011; 2:2047–2054. [PubMed: 21750779]
79. Diop M, Verdecchia K, Lee TY, St Lawrence K. Calibration of diffuse correlation spectroscopy with a time-resolved near-infrared technique to yield absolute cerebral blood flow measurements. Biomed. Opt. Express. 2011; 2:2068–2081. [PubMed: 21750781]
80. Durduran T, Choe R, Yu G, Zhou C, Tchou JC, Czerniecki BJ, Yodh AG. Diffuse optical measurement of blood flow in breast tumors. Opt. Lett. 2005; 30:2915–2917. [PubMed: 16279468]
81. Busch, DR. Ph.D. Dissertation. University of Pennsylvania; 2011. Computer-aided, multi-modal, and compression diffuse optical studies of breast tissue.
82. Zhou C, Choe R, Shah N, Durduran T, Yu G, Durkin A, Hsiang D, Mehta R, Butler J, Cerussi A, Tromberg BJ, Yodh AG. Diffuse optical monitoring of blood flow and oxygenation in human breast cancer during early stages of neoadjuvant chemotherapy. J. Biomed. Opt. 2007; 12:051903. [PubMed: 17994886]
83. Choe, R.; Yodh, AG. Diffuse optical tomography of the breast. In: Suri, J.; Rangayyan, RM.; Laxminarayan, S., editors. Emerging Technologies in Breast Imaging and Mammography. American Scientific Publishers; 2007. p. 1-26.
84. Perini R, Choe R, Yodh AG, Sehgal C, Divgi C, Rosen MA. Non-invasive assessment of tumor neovasculature: Techniques and clinical applications. Cancer Metastasis Rev. 2008; 27:615–630. [PubMed: 18506398]
85. Cutler M. Transillumination of the breast. Surg. Gynecol. Obstet. 1929; 48:721–727.
86. Suzuki K, Yamashita Y, Ohta K, Kaneko M, Yoshida M, Chance B. Quantitative mesurement of optical parameters in normal breasts using time-resolved spectroscopy: In vivo results of 30 Japanese women. J. Biomed. Opt. 1996; 1:330–334. [PubMed: 23014733]
87. Chance B. Near-infrared images using continuous, phase-modulated, and pulsed light with quantitation of blood and blood oxygenation. Ann. N. Y. Acad. Sci. 1998; 838:19–45.
88. Shah N, Cerussi A, Eker C, Espinoza J, Butler J, Fishkin J, Hornung R, Tromberg B. Noninvasive functional optical spectroscopy of human breast tissue. Proc. Natl. Acad. Sci. U. S. A. 2001; 98:4420–4425. [PubMed: 11287650]
89. Durduran T, Choe R, Culver JP, Zubkov L, Holboke MJ, Giammarco J, Chance B, Yodh AG. Bulk optical properties of healthy female breast tissue. Phys. Med. Biol. 2002; 47:2847–2861. [PubMed: 12222850]
90. Jiang SD, Pogue BW, Paulsen KD, Kogel C, Poplack SP. In vivo near-infrared spectral detection of pressure-induced changes in breast tissue. Opt. Lett. 2003; 28:1212–1214. [PubMed: 12885024]
91. Srinivasan S, Pogue BW, Jiang SD, Dehghani H, Kogel C, Soho S, Gibson JJ, Tosteson TD, Poplack SP, Paulsen KD. Interpreting hemoglobin and water concentration, oxygen saturation, and scattering measured in vivo by near-infrared breast tomography. Proc. Natl. Acad. Sci. U. S. A. 2003; 100:12 349–12 354.

92. Spinelli L, Torricelli A, Pifferi A, Taroni P, Danesini GM, Cubeddu R. Bulk optical properties and tissue components in the female breast from multiwavelength time-resolved optical mammography. J. Biomed. Opt. 2004; 9:1137–1142. [PubMed: 15568933]

93. Taroni P, Bassi A, Comelli D, Farina A, Cubeddu R, Pifferi A. Diffuse optical spectroscopy of breast tissue extended to 1100 nm. J. Biomed. Opt. 2009; 14:054030. [PubMed: 19895132]

94. Fang Q, Carp SA, Selb J, Boverman G, Zhang Q, Kopans DB, Moore RH, Miller EL, Brooks DH, Boas DA. Combined optical imaging and mammography of the healthy breast: optical contrast derived from breast structure and compression. IEEE Trans. Med. Imaging. 2009; 28:30–42. [PubMed: 19116186]

95. Blyschak K, Simick M, Jong R, Lilge L. Classification of breast tissue density by optical transillumination spectroscopy: Optical and physiological effects governing predictive value. Med. Phys. 2004; 31:1398–1414. [PubMed: 15259643]

96. Blackmore KM, Knight JA, Jong R, Lilge L. Assessing breast tissue density by transillumination breast spectroscopy (tibs): an intermediate indicator of cancer risk. British Journal Of Radiology. 2007; 80:545–556. [PubMed: 17537757]

97. Blackmore KM, Knight JA, Lilge L. Association between transillumination breast spectroscopy and quantitative mammographic features of the breast. Cancer Epidemiology Biomarkers & Prevention. 2008; 17:1043–1050.

98. Taroni P, Pifferi A, Quarto G, Spinelli L, Torricelli A, Abbate F, Villa A, Balestreri N, Menna S, Cassano E, Cubeddu R. Noninvasive assessment of breast cancer risk using time-resolved diffuse optical spectroscopy. J. Biomed. Opt. 2010; 15:060501. [PubMed: 21198142]

99. Choe R, Konecky SD, Corlu A, Lee K, Durduran T, Busch DR, Czerniecki BJ, Tchou J, Fraker DL, DeMichele A, Chance B, Arridge SR, Schweiger M, Culver JP, Schnall MD, Putt ME, Rosen MA, Yodh AG. Differentiation of benign and malignant breast tumors by in-vivo three-dimensional parallel-plate diffuse optical tomography. J. Biomed. Opt. 2009; 14(2):024020. [PubMed: 19405750]

100. Fang Q, Selb J, Carp SA, Boverman G, Miller EL, Brooks DH, Moore RH, Kopans DB, Boas DA. Combined optical and x-ray tomosynthesis breast imaging. Radiology. 2011; 258:89–97. [PubMed: 21062924]

101. Ntziachristos V, Yodh AG, Schnall M, Chance B. Concurrent MRI and diffuse optical tomography of breast after indocyanine green enhancement. Proc. Natl. Acad. Sci. U. S. A. 2000; 97:2767–2772. [PubMed: 10706610]

102. Intes X, Ripoll J, Chen Y, Nioka S, Yodh AG, Chance B. In vivo continuous-wave optical breast imaging enhanced with indocyanine green. Med. Phys. 2003; 30:1039–1047. [PubMed: 12852527]

103. Corlu A, Choe R, Durduran T, Rosen MA, Schweiger M, Arridge SR, Schnall MD, Yodh AG. Three-dimensional in vivo fluorescence diffuse optical tomography of breast cancer in humans. Opt. Express. 2007; 15:6696–6716. [PubMed: 19546980]

104. Hagen A, Grosenick D, Macdonald R, Rinneberg H, Burock S, Warnick P, Poellinger A, Schlag PM. Late-fluorescence mammography assesses tumor capillary permeability and differentiates malignant from benign lesions. Opt. Express. 2009; 17:17 016–17 033.

105. Poellinger A, Burock S, Grosenick D, Hagen A, Lüdemann L, Diekmann F, Engelken F, Macdonald R, Rinneberg H, Schlag P. Breast cancer: early- and late-fluorescence near-infrared imaging with Indocyanine Green - a preliminary study. Radiology. 2010; 258:409–416. [PubMed: 21177396]

106. Grosenick D, Hagen A, Steinkellner O, Poellinger A, Burock S, Schlag PM, Rinneberg H, Macdonald R. A multichannel time-domain scanning fluorescence mammo-graph: performance assessment and first in vivo results. Rev. Sci. Inst. 2011; 82:024302.

107. Jakubowski DB, Cerussi AE, Bevilacqua F, Shah N, Hsiang D, Butler J, Tromberg BJ. Monitoring neoadjuvant chemotherapy in breast cancer using quantitative diffuse optical spectroscopy: a case study. J. Biomed. Opt. 2004; 9:230–238. [PubMed: 14715078]

108. Choe R, Corlu A, Lee K, Durduran T, Konecky SD, Grosicka-Koptyra M, Arridge SR, Czerniecki BJ, Fraker DL, DeMichele A, Chance B, Rosen MA, Yodh AG. Diffuse optical

tomography of breast cancer during neoadjuvant chemotherapy: a case study with comparison to MRI. Med. Phys. 2005; 32(4):1128–1139. [PubMed: 15895597]

109. Shah N, Gibbs J, Wolverton D, Cerussi A, Hylton N, Tromberg BJ. Combined diffuse optical spectroscopy and contrast-enhanced magnetic resonance imaging for monitoring breast cancer neoadjuvant chemotherapy: a case study. J. Biomed. Opt. 2005; 10:051503. [PubMed: 16292947]
110. Tromberg BJ, Cerussi A, Shah N, Compton M, Durkin A, Hsiang D, Butler J, Mehta R. Diffuse optics in breast cancer: detecting tumors in pre-menopausal women and monitoring neoadjuvant chemotherapy. Breast Cancer Res. 2005; 7:279–285. [PubMed: 16457705]
111. Zhu Q, Kurtzma SH, Hegde P, Tannenbaum S, Kane M, Huang M, Chen NG, Jagjivan B, Zarfos K. Utilizing optical tomography with ultrasound localization to image heterogeneous hemoglobin distribution in large breast cancers. Neoplasia. 2005; 7:263–270. [PubMed: 15799826]
112. Cerussi A, Hsiang D, Shah N, Mehta R, Durkin A, Butler J, Tromberg BJ. Predicting response to breast cancer neoadjuvant chemotherapy using diffuse optical spectroscopy. Proc. Natl. Acad. Sci. U. S. A. 2007; 104:4014–4019. [PubMed: 17360469]
113. Zhu Q, Tannenbaum S, Hegde P, Kane M, Xu C, Kurtzman SH. Noninvasive monitoring of breast cancer during neoadjuvant chemotherapy using optical tomography with ultrasound localization. Neoplasia. 2008; 10:1028–1040. [PubMed: 18813360]
114. Jiang S, Pogue BW, Carpenter CM, Poplack SP, Wells WA, Kogel CA, Forero JA, Muffly LS, Schwartz GN, Paulsen KD, Kaufman PA. Evaluation of breast tumor response to neoadjuvant chemotherapy with tomographic diffuse optical spectroscopy: Case studies of tumor region-of-interest changes. Radiology. 2009; 252:551–560. [PubMed: 19508985]
115. Soliman H, Gunasekara A, Rycroft M, Zubovits J, Dent R, Spayne J, Yaffe MJ, Czarnota GJ. Functional imaging using diffuse optical spectroscopy of neoadjuvant chemotherapy response in women with locally advanced breast cancer. Clin. Cancer Res. 2010; 16:2605–2614. [PubMed: 20406836]
116. Cerussi AE, Tanamai VW, Mehta RS, Hsiang D, Butler J, Tromberg BJ. Frequent optical imaging during breast cancer neoadjuvant chemotherapy reveals dynamic tumor physiology in an individual patient. Acad. Radiol. 2010; 17:1031–1039. [PubMed: 20542448]
117. Roblyer D, Ueda S, Cerussi A, Tanamai W, Durkin A, Mehta R, Hsiang D, Butler JA, McLaren C, Chen WP, Tromberg B. Optical imaging of breast cancer oxy-hemoglobin flare correlates with neoadjuvant chemotherapy response one day after starting treatment. Proc. Natl. Acad. Sci. U. S. A. 2011; 108:14 626–14 631.
118. Cerussi AE, Tanamai VW, Hsiang D, Butler J, Mehta RS, Tromberg BJ. Diffuse optical spectroscopic imaging correlates with final pathological response in breast cancer neoadjuvant chemotherapy. Phil. Trans. R. Soc. A. 2011; 369:4512–4530. [PubMed: 22006904]
119. Hebden JC, Yates TD, Gibson A, Everdell N, Arridge SR, Chicken DW, Douek M, Keshtgar MRS. Monitoring recovery after laser surgery of the breast with optical tomography: a case study. Appl. Opt. 2005; 44(10):1898–1904. [PubMed: 15813526]
120. Tanamai W, Chen C, Siavoshi S, Cerussi A, Hsiang D, Butler J, Tromberg B. Diffuse optical spectroscopy measurements of healing in breast tissue after core biopsy: case study. J. Biomed. Opt. 2009; 14:014024. [PubMed: 19256712]
121. Sevick-Muraca EM, Sharma R, Rasmussen JC, Marshall MV, Wendt JA, Pham HQ, Bonefas E, Houston JP, Sampath L, Adams KE, Blanchard DK, Fisher RE, Chiang SB, Elledge R, Mawad ME. Imaging of lymph flow in breast cancer patients after microdose administration of a near-infrared fluorophore: Feasibility study. Radiology. 2008; 246:734–741. [PubMed: 18223125]
122. Hutteman M, Mieog JS, van der Vorst JR, Liefers GJ, Putter H, Löwik CW, Frangioni JV, van de Velde CJ, Vahrmeijer AL. Randomized, double-blind comparison of indocyanine green with or without albumin premixing for near-infrared fluorescence imaging of sentinel lymph nodes in breast cancer patients. Breast Cancer Res. Treat. 2011; 127:163–170. [PubMed: 21360075]
123. Jiang HB, Iftimia NV, Xu Y, Eggert JA, Fajardo LL, Klove KL. Near-infrared optical imaging of the breast with model-based reconstruction. Acad. Radiol. 2002; 9:186–194. [PubMed: 11918371]
124. Chance B, Nioka S, Zhang J, Conant EF, Hwang E, Briest S, Orel SG, Schnall MD, Czerniecki BJ. Breast cancer detection based on incremental biochemical and physiological properties of

breast cancers: A six-year, two-site study. Acad. Radiol. 2005; 12:925–933. [PubMed: 16023383]

125. Intes X, Djeziri S, Ichalalene Z, Mincu N, Wang Y, St-Jean P, Lesage F, Hall D, Boas D, Polyzos M, Fleiszer D, Mesurolle B. Time-domain optical mammography SoftScan: Initial results. Acad. Radiol. 2005; 12:934–947. [PubMed: 16023382]
126. Zhu Q, Cronin EB, Currier AA, Vine HS, Huang M, Chen N, Xu C. Benign versus malignant breast masses: Optical differentiation with US-guided optical imaging reconstruction. Radiology. 2005; 237:57–66. [PubMed: 16183924]
127. Grosenick D, Wabnitz H, Moesta KT, Mucke J, Schlag PM, Rinneberg H. Time-domain scanning optical mammography: II. Optical properties and tissue parameters of 87 carcinomas. Phys. Med. Biol. 2005; 50(11):2451–2468. [PubMed: 15901948]
128. Xu RX, Young DC, Mao JJ, Povoski SP. A prospective pilot clinical trial evaluating the utility of a dynamic near-infrared imaging device for characterizing suspicious breast lesions. Breast Cancer Res. 2007; 9:R88. [PubMed: 18088411]
129. Poplack SP, Tosteson TD, Wells WA, Pogue BW, Meaney PM, Hartov A, Kogel CA, Soho SK, Gibson JJ, Paulsen KD. Electromagnetic breast imaging: Results of a pilot study in women with abnormal mammograms. Radiology. 2007; 243(2):350–359. [PubMed: 17400760]
130. Cerussi A, Shah N, Hsiang D, Durkin A, Butler J, Tromberg BJ. In vivo absorption, scattering, and physiologic properties of 58 malignant breast tumors determined by broadband diffuse optical spectroscopy. J. Biomed. Opt. 2006; 11:044005. [PubMed: 16965162]
131. Enfield LC, Gibson AP, Everdell NL, Delpy DT, Schweiger M, Arridge SR, Richardson C, Keshtgar M, Douek M, Hebden JC. Three-dimensional time-resolved optical mammography of the uncompressed breast. Appl. Opt. 2007; 46:3628–3638. [PubMed: 17514325]
132. Pogue BW, Poplack SP, McBride TO, Wells WA, Osterman KS, Osterberg UL, Paulsen KD. Quantitative hemoglobin tomography with diffuse near-infrared spectroscopy: Pilot results in the breast. Radiology. 2001; 218:261–266. [PubMed: 11152812]
133. Srinivasan S, Pogue BW, Brooksby B, Jiang S, Dehghani H, Kogel C, Wells WA, Poplack SP, Paulsen KD. Near-infrared characterization of breast tumors in vivo using spectrally-constrained reconstruction. Tech. Cancer Res. Treat. 2005; 4:513–526.
134. Tromberg BJ, Shah N, Lanning R, Cerussi A, Espinoza J, Pham T, Svaasand L, Butler J. Non-invasive in vivo characterization of breast tumors using photon migration spectroscopy. Neoplasia. 2000; 2:26–40. [PubMed: 10933066]
135. Chung SH, Cerussi AE, Klifa C, Baek HM, Birgul O, Gulsen G, Merritt SI, Hsiang D, Tromberg BJ. In vivo water state measurements in breast cancer using broadband diffuse optical spectroscopy. Phys. Med. Biol. 2008; 53:6713–6727. [PubMed: 18997265]
136. Taroni P, Comelli D, Pifferi A, Torricelli A, Cubeddu R. Absorption of collagen: effects on the estimate of breast composition and related diagnostic implications. J. Biomed. Opt. 2007; 12:014021. [PubMed: 17343496]
137. Liang X, Zhang Q, Li C, Grobmyer SR, Fajardo LL, Jiang H. Phase-contrast diffuse optical tomography: Pilot results in the breast. Acad. Radiol. 2008; 15:859–866. [PubMed: 18572121]
138. Wang JZ, Liang X, Zhang Q, Fajardo LL, Jiang H. Automated breast cancer classification using near-infrared optical tomographic images. J. Biomed. Opt. 2008; 13:044001. [PubMed: 19021329]
139. Sevick-Muraca EM, Rasmussen JC. Molecular imaging with optics: primer and case for near-infrared fluorescence techniques in personalized medicine. J. Biomed. Opt. 2008; 13:041303. [PubMed: 19021311]
140. Reynolds JS, Troy TL, Mayer RH, Thompson AB, Waters DJ, Cornell KK, Snyder PW, Sevick-Muraca EM. Imaging of spontaneous canine mammary tumors using fluorescent contrast agents. Photochem. Photobiol. 1999; 70:87–94. [PubMed: 10420847]
141. Godavarty A, Eppstein MJ, Zhang CY, Theru S, Thompson AB, Gurfinkel M, Sevick-Muraca EM. Fluorescence-enhanced optical imaging in large tissue volumes using a gain-modulated ICCD camera. Phys. Med. Biol. 2003; 48:1701–1720. [PubMed: 12870578]

142. Leblond F, David SC, Valdés PA, Pogue BW. Pre-clinical whole-body fluorescence imaging: Review of instruments, methods and applications. J. Photochem. Photobiol. B. 2010; 98:77–94. [PubMed: 20031443]

143. Bastiaens PI, Squire A. Fluorescence lifetime imaging microscopy: spatial resolution of biochemical processes in the cell. Trends Cell Biol. 1999; 9:48–52. [PubMed: 10087617]

144. Kuwana E, Sevick-Muraca EM. Fluorescence lifetime spectroscopy for pH sensing in scattering media. Anal. Chem. 2003; 75:4325–4329. [PubMed: 14632153]

145. Boas, DA.; Pitris, C.; Ramanujam, N., editors. Handbook of Biomedical Optics. CRC Press; Boca Raton: 2011.

146. Wang, LV.; Wu, HI. Biomedical Optics: Principles and Imaging. John Wiley & Sons, Inc.; New Jersey: 2007.

147. Wang LV. Tutorial on photoacoustic microscopy and computed tomography. IEEE J. Sel. Top. Quantum Electron. 2008; 14:171–179.

148. Bardhan R, Chen W, Bartels M, Perez-Torres C, Botero MF, McAninch RW, Contreras A, Schiff R, Pautler RG, Halas NJ, Joshi A. Tracking of multimodal therapeutic nanocomplexes targeting breast cancer in vivo. Nano Lett. 2010; 10:4920–4928.

149. Carpenter CM, Pogue BW, Jiang S, Dehghani H, Wang X, Paulsen KD, Wells WA, Forero J, Kogel C, Weaver JB, Poplack SP, Kaufman PA. Image-guided optical spectroscopy provides molecular-specific information in vivo: MRI-guided spectroscopy of breast cancer hemoglobin, water, and scatterer size. Opt. Lett. 2007; 32:933–935. [PubMed: 17375158]

150. Wang J, Davis SC, Srinivasan S, Jiang S, Pogue BW, Paulsen KD. Spectral tomography with diffuse near-infrared light: inclusion of broadband frequency domain spectral data. J. Biomed. Opt. 2008; 13:041305. [PubMed: 19021313]

151. Wang J, Jiang S, Li Z, diFlorio-Alexander RM, Barth RJ, Kaufman PA, Pogue BW, Paulsen KD. In vivo quantitative imaging of normal and cancerous breast tissue using broadband diffuse optical tomography. Med. Phys. 2011; 37:3715–3724. [PubMed: 20831079]

152. Bevilacqua F, Berger AJ, Cerussi AE, Jakubowski D, Tromberg BJ. Broadband absorption spectroscopy in turbid media by combined frequency-domain and steady-state methods. Appl. Opt. 2000; 39:6498–6507. [PubMed: 18354663]

153. Cheung C, Culver JP, Takahashi K, Greenberg JH, Yodh AG. In vivo cerebrovascular measurement combining diffuse near-infrared absorption and correlation spectroscopies. Phys. Med. Biol. 2001; 46:2053–2065. [PubMed: 11512610]

154. Li J, Dietsche G, Iftime D, Skipetrov SE, Maret G, Elbert T, Rockstroh B, Gisler T. Noninvasive detection of functional brain activity with near-infrared diffusing-wave spectroscopy. J. Biomed. Opt. 2005; 10:044002.

155. Zirak P, Delgado-Mederos R, Martí–Fàbregas J, Durduran T. Effects of acetazolamide on the micro- and macro-vascular cerebral hemodynamics: A diffuse optical and transcranial doppler ultrasound study. Biomed. Opt. Express. 2010; 1:1443–1459. [PubMed: 21258561]

156. Sunar U, Rohrbach D, Rigual N, Tracy E, Keymel K, Cooper MT, Baumann H, Henderson BH. Monitoring photobleaching and hemodynamic responses to HPPH-mediated photodynamic therapy of head and neck cancer: a case report. Opt. Express. 2010; 18:14 969–14 978.

157. Shang Y, Zhao Y, Cheng R, Dong L, Irwin D, Yu G. Portable optical tissue flow oximeter based on diffuse correlation spectroscopy. Opt. Lett. 2009; 34:3556–3558. [PubMed: 19927209]

158. Carp SA, Dai GP, Boas DA, Franceschini MA, Kim YR. Validation of diffuse correlation spectroscopy measurements of rodent cerebral blood flow with simultaneous arterial spin labeling MRI; towards MRI-optical continuous cerebral metabolic monitoring. Biomed. Opt. Express. 2010; 1:553–565. [PubMed: 21258489]

159. Durduran, T. Ph.D. dissertation. University of Pennsylvania; 2004. Non-invasive measurements of tissue hemodynamics with hybrid diffuse optical methods.

160. Zhou, C. Ph.D. dissertation. University of Pennsylvania; 2007. In-vivo optical imaging and spectroscopy of cerebral hemodynamics.

161. Corlu A, Durduran T, Choe R, Schweiger M, Hillman EMC, Arridge SR, Yodh AG. Uniqueness and wavelength optimization in continuous-wave multispectral diffuse optical tomography. Opt. Lett. 2003; 28:2339–2341. [PubMed: 14680175]

162. Corlu A, Choe R, Durduran T, Lee K, Schweiger M, Arridge SR, Hillman EMC, Yodh AG. Diffuse optical tomography with spectral constraints and wavelength optimization. Appl. Opt. 2005; 44(11):2082–2093. [PubMed: 15835357]

163. Franceschini MA, Moesta KT, Fantini S, Gaida G, Gratton E, Jess H, Mantulin WW, Seeber M, Schlag PM, Kaschke M. Frequency-domain techniques enhance optical mammography: Initial clinical results. Proc. Natl. Acad. Sci. U. S. A. 1997; 94:6468–6473. [PubMed: 9177241]

164. Grosenick D, Wabnitz H, Rinneberg HH, Moesta KT, Schlag PM. Development of a time-domain optical mammograph and first in vivo applications. Appl. Opt. 1999; 38:2927–2943. [PubMed: 18319875]

165. Heffer E, Pera V, Schutz O, Siebold H, Fantini S. Near-infrared imaging of the human breast: complementing hemoglobin concentration maps with oxygenation images. J. Biomed. Opt. 2004; 9:1152–1160. [PubMed: 15568935]

166. Grosenick D, Moesta KT, Möller M, Mucke J, Wabnitz H, Gebauer B, Stroszczynski C, Wassermann B, Schlag PM, Rinneberg H. Time-domain scanning optical mammography: I. Recording and assessment of mammograms of 154 patients. Phys. Med. Biol. 2005; 50(11): 2429–2450. [PubMed: 15901947]

167. Taroni P, Torricelli A, Spinelli L, Pifferi A, Arpaia F, Danesini G, Cubeddu R. Time-resolved optical mammography between 637 and 985 nm: clinical study on the detection and identification of breast lesions. Phys. Med. Biol. 2005; 50(11):2469–2488. [PubMed: 15901949]

168. Spinelli L, Torricelli A, Pifferi A, Taroni P, Danesini G, Cubeddu R. Characterization of female breast lesions from multi-wavelength time-resolved optical mammography. Phys. Med. Biol. 2005; 50(11):2489–2502. [PubMed: 15901950]

169. Yu Y, Liu N, Sassaroli A, Fantini S. Near-infrared spectral imaging of the female breast for quantitative oximetry in optical mammography. Appl. Opt. 2009; 48:D225–235. [PubMed: 19340113]

170. Dierkes T, Grosenick D, Moesta KT, Möller M, Schlag PM, Rinneberg H, Arridge S. Reconstruction of optical properties of phantom and breast lesion in vivo from paraxial scanning data. Phys. Med. Biol. 2005; 50(11):2519–2542. [PubMed: 15901952]

171. McBride TO, Pogue BW, Jiang S, Osterberg UL, Paulsen KD. A parallel-detection frequency-domain near-infrared tomography system for hemoglobin imaging of the breast in vivo. Rev. Sci. Instrum. 2001; 72:1817–1824.

172. Jiang H, Paulsen KD, Osterberg UL, Pogue BW, Patterson MS. Optical image reconstruction using frequency-domain data: simulations and experiments. J. Opt. Soc. Am. A. 1996; 13(2): 253–266.

173. Pogue BW, McBride TO, Prewitt J, Osterberg UL, Paulsen KD. Spatially variant regularization improves diffuse optical tomography. Appl. Opt. 1999; 38:2950–2961. [PubMed: 18319877]

174. Davis, SC.; Mastanduno, MA.; Pogue, BW.; Paulsen, KD. SPIE Photonics West. Vol. 7892. San Francisco, CA: 2011. MRI-guided fluorescence tomography of PPIX in the breast: A case study; p. 78920M

175. Zhu QI, Huang MM, Chen NG, Zarfos K, Jagjivan B, Kane M, Hedge P, Kurtzman SH. Ultrasound-guided optical tomographic imaging of malignant and benign breast lesions: Initial clinical results of 19 cases. Neoplasia. 2003; 5:379–388. [PubMed: 14670175]

176. Baselga J. New therapeutic agents targeting the epidermal growth factor receptor. J. Clinc. Oncol. 2000; 18:54s–59s.

177. Cerniglia GJ, Pore N, Tsai JH, Schultz S, Mick R, Choe R, Xing X, Durduran T, Yodh AG, Evans SM, Koch CJ, Hahn SM, Quon H, Sehgal CM, Lee WMF, Maity A. Epidermal growth factor receptor inhibition modulates the microenvironment by vascular normalization to improve chemotherapy and radiotherapy e cacy. PLoS One. 2009; 4:e6539. [PubMed: 19657384]

178. Busch DR, Guo W, Choe R, Durduran T, Feldman MD, Mies C, Rosen MA, Schnall MD, Czerniecki BJ, Tchou J, DeMichele A, Putt ME, Yodh AG. Computer aided automatic detection of malignant lesions in diffuse optical mammography. Med. Phys. 2010; 37:1840–1849. [PubMed: 20443506]

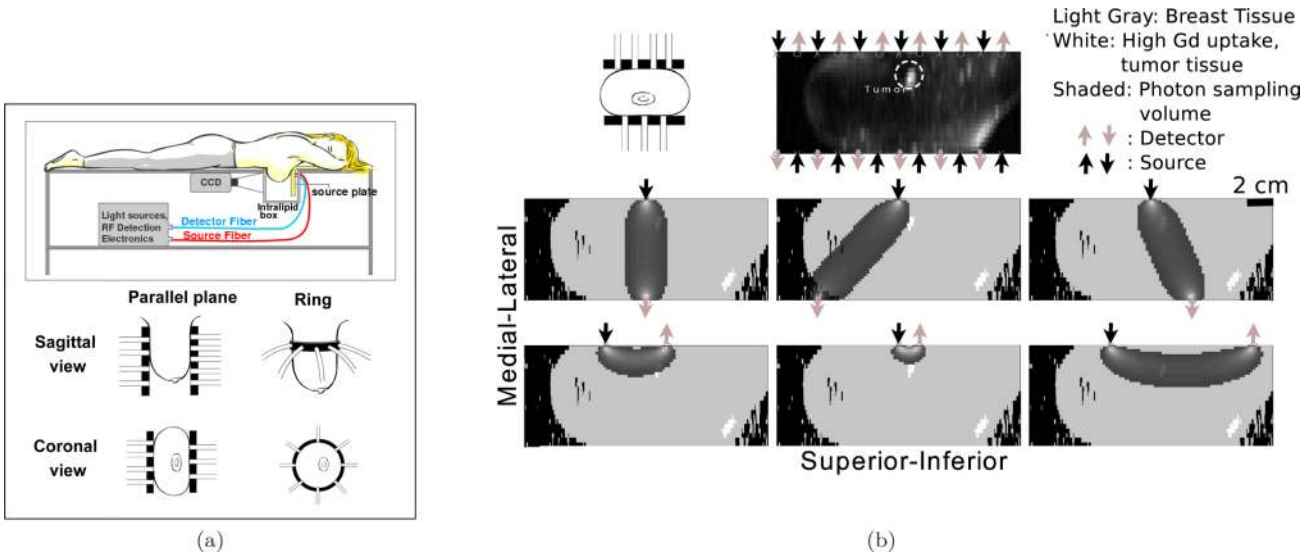

Fig. 1.

(a) A sketch of the University of Pennsylvania system (DOT-3) is shown as a representative stand-alone DOT system. Different views of parallel-plate data-acquisition and circular data-acquisition (DOT-5) schemes are also illustrated. In most stand-alone tomographic systems, the subject lies in the prone position. (b) A series of figures demonstrating photon propagation in the female breast and the importance of physical modeling. Top-middle: A DCE-MRI scan showing high uptake in the tumor region and an image artifact (bottom right of the image) with a "generic" set of sources (dark arrows) and detectors (light arrows) indicated in two parallel plates that are in contact with the breast. A mask was applied indicating high contrast agent uptake ("white"), the breast tissue ("light gray") and elsewhere ("black") which is shown in the bottom two rows. Middle-row shows a series of transmission measurements and a map of the photon-visiting probability of >95% (for better visualization) overlaid. Bottom-row shows similar information for reflectance (or re-emission) measurements.

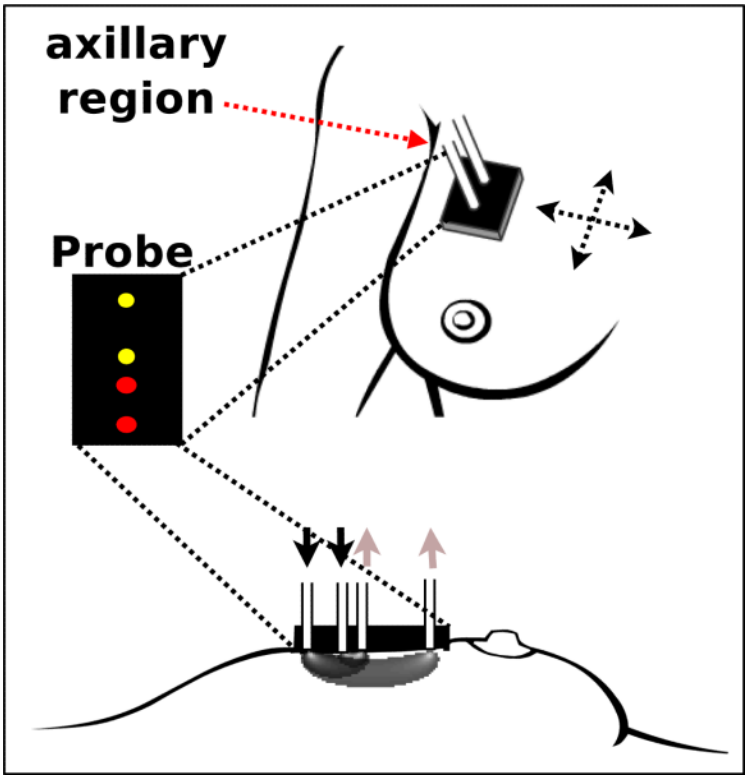

Fig. 2.

(Top) A sketch of a generic reflectance probe is shown as a representative hand-held system. A probe with several source-detector pairs and sometimes the parts of another modality (e.g., ultrasound as in the US/DOT-6) is scanned across several locations of the breast. (Bottom) An illustration demonstrates the relationship between the probed depth and the source-detector separation. A map of the photon-visiting probability of >95% is overlaid on the breast tissue, where sources (dark arrow) and detectors (light arrow) are indicated. Notice the differences in the breast-volume/shape between Figure 1a and this approach where the subject lies in the supine position, thus, flattening the breast.

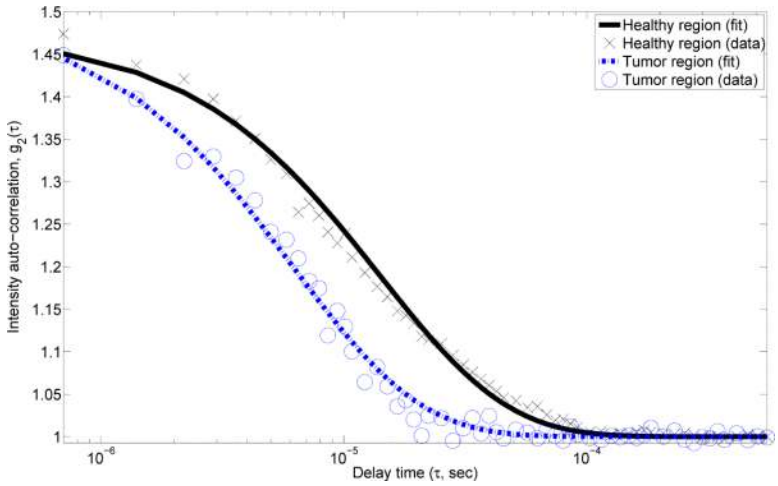

Fig. 3.

The intensity auto-correlation functions measured from a “healthy” and from a “tumor” region are shown with semi-infinite fits overlaid. The faster decay of the curves in the tumor region correspond to increased *BF* flow by a factor of ~2.3 when compared to that of the healthy region.

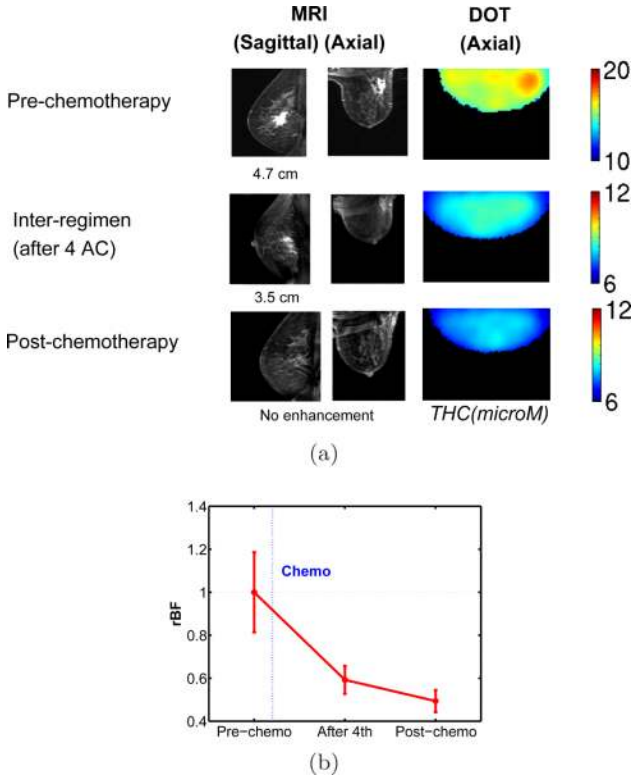

Fig. 4.

An example of diffuse optical tomography (DOT) and diffuse correlation spectroscopy (DCS) applied for chemotherapy monitoring of a complete pathologic responder. (a) Dynamic-contrast-enhanced MRI shows dramatic tumor size shrinkage as the therapy progresses. Well-localized high total hemoglobin concentration region corresponding to the tumor at pre-chemotherapy time point becomes homogeneous as the therapy progresses. (b) Relative blood flow $rBF = BF/BF_{pre}$ at tumor region decreases with the therapy progress. (Figure is in color.)

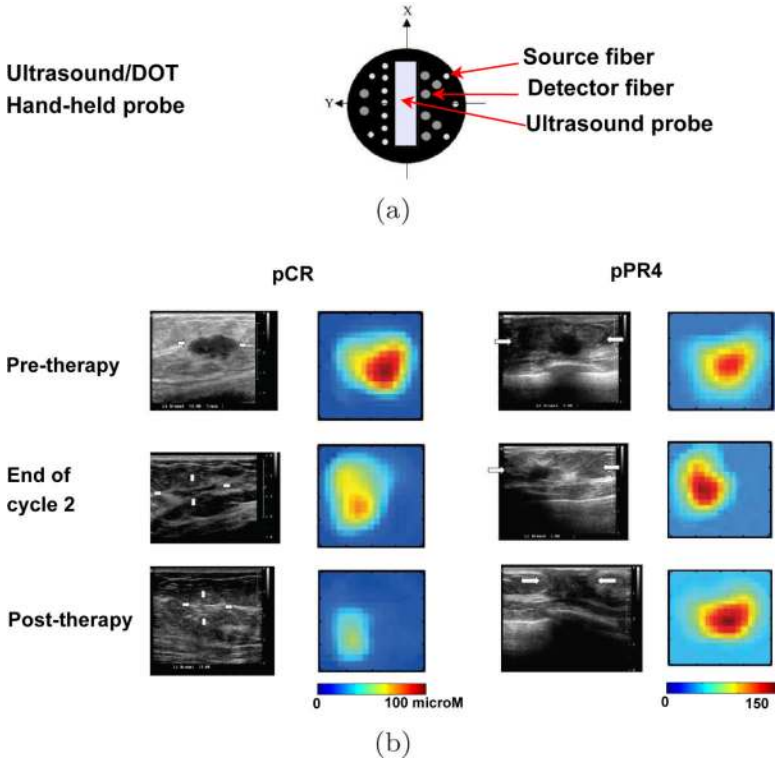

Fig. 5.

(a) A hand-held probe combining ultrasound transducer and optical fibers used in US/DOT-6 system, (b) Selected slice of ultrasound image and multi-modal DOT image at pre-therapy, end of cycle 2 and post-therapy time points arranged from top to bottom. Left set shows images from a responding patient, whereas right set shows images from a non-responding patient. Figures are adapted with permission from [113], [175]. (Figure is in color.)

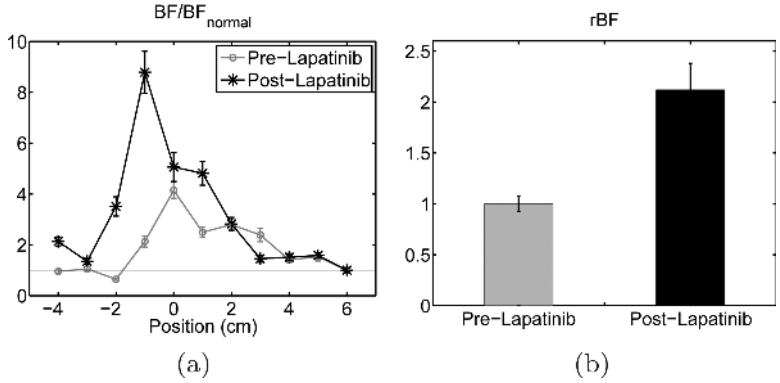

Fig. 6.

Blood flow variations induced by Lapatinib therapy. (a) Line scans of *BF* normalized with normal tissue in tumor-bearing breast show enhanced blood flow between -1 and 0 cm, which corresponds to tumor center at both pre- and post-therapy time points. (b) $rBF = BF/BF_{pre}$ at tumor region shows increase after Lapatinib therapy.

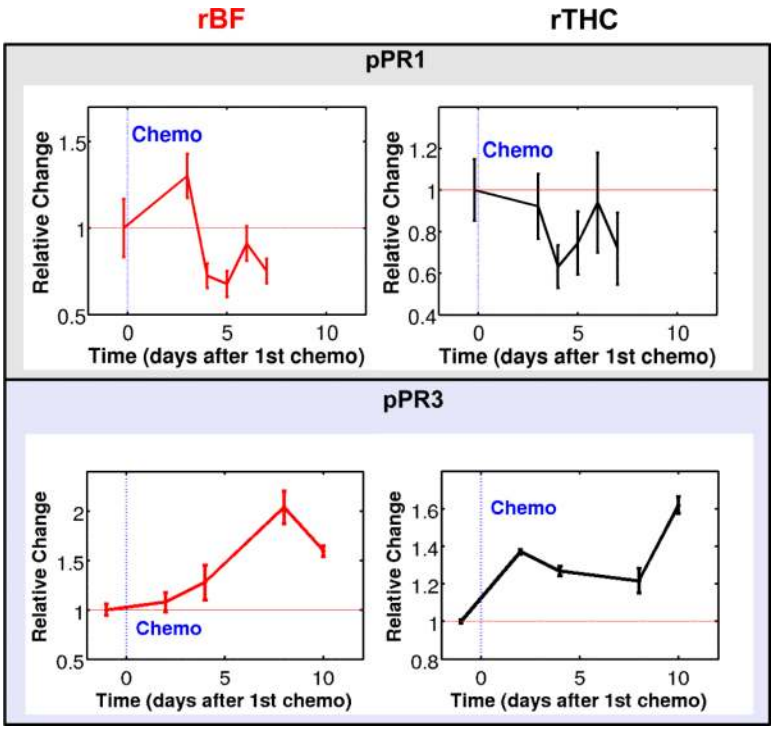

Fig. 7.
Different dynamic response may distinguish the degree of responses in partial responders. pPR1 case is adapted with permission from [82].

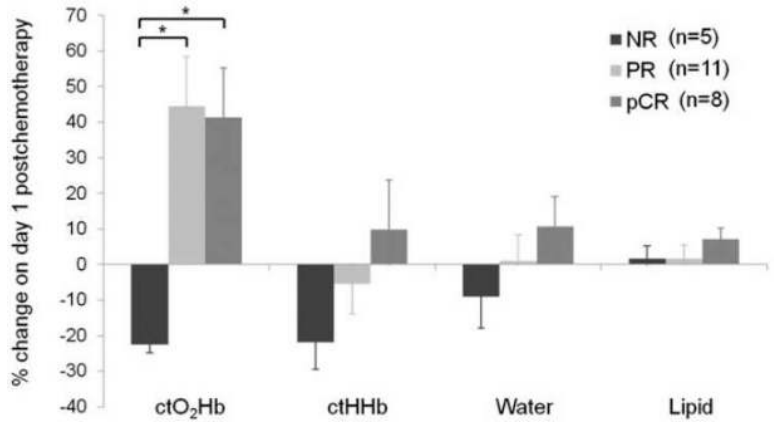

Fig. 8.

Percent change in HbO_2 (ctO_2Hb), Hb ($ctHHb$), water and lipid on day 1 compared with baseline. Non-responder (NR) in this classification contains pPR3 and pPR4 categories, whereas partial responder (PR) contains pPR1 and pPR2 categories. Oxyhemoglobin flare on day 1 distinguishes non-responding group from the rest (i.e., pCR and pPR1,2). Reproduced with permission from [117].

TABLE I

List of diffuse optical systems and the reported physiological parameters as they were applied for neoadjuvant chemotherapy monitoring. The measurable parameters tend to differ among systems depending on the capabilities of each system. In section IV-A, we discuss each system in details. (UCI: University of California, Irvine; UPENN: University of Pennsylvania, ART: Advanced Research Technologies Inc., Dartmouth: Dartmouth College, UConn: University of Connecticut)

Group	System	Parameters
UCI	DOS-1	*Hb, HbO_2, H_2O, Lipid, A, b*
UPENN	DCS-2	*BF*
UPENN	DOT-3	*Hb, HbO_2, b*
ART	DOT-4	*Hb, HbO_2, H_2O, b*
Dartmouth	DOT-5	*Hb, HbO_2, H_2O, A, b*
UConn	US/DOT-6	*Hb, HbO_2*

TABLE II

Case studies demonstrating that diffuse optics can track changes induced by chemotherapy and/or targeted therapy. Systems are denoted with the convention introduced in section IV-A. The time points are heterogeneous, ranging from short-term (daily) to long-term (months). Note that each row corresponds to information of one patient. (N/A = Not available)

Reference	System	Therapy	Response	Time points
Jakubowski *et al* [107]	DOS-1	*AC*	pPR2	pre, days 3,4,5,6,7 (after 1st *AC*), 26, 28 days (after 2nd *AC*), post
Shah *et al* [109]	DOS-1	*AC*→*T*	pPR3	2 weeks after 1st *AC*, mid-therapy
Tromberg *et al* [110]	DOS-1	*AC*	N/A	pre, 1,2,3,6,8 days after 1st *AC*
Cerussi *et al* [116]	DOS-1	*AC*→Bevacizumab	pPR1	pre, 20 time points throughout the therapy
Zhou *et al* [82]	DCS-2, DOS-1	*AC*	pPR1	pre, 3,4,5,6,7 days after 1st *AC*
Choe *et al* [108]	DOT-3	*AC*→*T*	pPR2	after 4, 5, 7 cycles
Zhu *et al* [111]	US/DOT-5	N/A	N/A	pre, post-therapy
		N/A	pPR1	pre, after 4, and 8 cycles

TABLE III

Feasibility studies demonstrating that the diffuse optics can predict therapy response. Systems are denoted with the convention introduced in section IV-A. Group 1 and Group 2 corresponds roughly to the responding and the non-responding group respectively. Under Group 1 and 2, the number of patients in the group and their pathologic response is shown in parenthesis – following our classification scheme described in section II. In addition to the information of diffuse optics measurement time points, the optimal time and the predictors are identified.

Reference	System	Group 1	Group 2	Time points	Optimal time	Predictors
Cerussi *et al* [112]	DOS-1	6 (pCR+pPRl,2)	5 (pPR3,4)	pre, 1 week after	1 week after	*Hb, HbO_2, H_2O*
Roblyer *et al* [117]	DOS-1	19 (pCR+pPRl,2)	5 (pPR3,4)	pre, 1-7 days	1 day after	HbO_2 flare
Cerussi *et al* [118]	DOS-1	11 (pCR)	25 (pPRl,2,3,4)	pre, mid, post	mid	*TOI*
					post	*TOI, Hb*
Soliman *et al* [115]	DOT-4	5 (pPR2)	3 (pPR3,4)	pre, 1, 4, 8 weeks after, post	4 week after	*Hb, HbO_2, b*
Jiang *et al* [114]	DOT-5	4 (pCR)	3 (pPRl,2,3,4)	pre, unspecified during, post	within 4 week	*THC*
Pakalniskis *et al* [44]	DOT-5	7 (pCR)	4 (pPRl,2)	pre, unspecified during, post	post	*THC*
Zhu *et al* [113]	US/DOT-6	7 (pCR+pPRl,2)	4(pPR3,4)	pre, 2,4,6 cycles, post	after 2nd cycle	% BVI